Fermi-liquid theory for thin arbitrarily polarized ^{3}He films

David Z. Li,* R. H. Anderson,† and M. D. Miller‡
Department of Physics and Astronomy, Washington State University, Pullman, Washington 99164-2814, USA
(Received 4 April 2012; revised manuscript received 23 May 2012; published 8 June 2012)

We study the thermodynamic response, effective masses, and collective excitations for thin (submonolayer) ^{3}He films as a function of density and polarization using Fermi liquid theory. The Landau parameters $f^{\uparrow\uparrow}, f^{\uparrow\downarrow}, f^{\downarrow\downarrow}$ are obtained to quadratic order in the low-density s-wave and p-wave T-matrix interaction parameters. Values for the effective interaction components are determined by fitting zero-polarization experimental data for the cases of thin ^{3}He films on graphite and also thin ^{3}He films in surface states of thin superfluid ^{4}He films. By fitting the interaction parameters, we can calculate the Landau parameters to all orders, and we show results for the behavior of $\tilde{F}_\ell^{\uparrow\uparrow}$ for $\ell \leqslant 30$. With knowledge of the Landau parameters we calculate the polarization dependence of the state-dependent effective masses, compressibility, spin susceptibility, and zero-sound spectra for the mobile submonolayer range of areal densities. Our results predict a dramatic decrease in the effective masses for ^{3}He on graphite as a function of polarization at higher coverages. At fixed density, the compressibility is shown to decrease monotonically with increasing polarization. At small polarization the inverse spin susceptibility is largest for small density whereas at large polarization it is largest for large density. We show that zero sound will propagate at all densities and polarizations whereas spin zero sound does not propagate in these systems. The condition for thermodynamic stability in an arbitrarily polarized Fermi liquid film is derived and discussed. We show explicitly the Fermi surface distortion due to the presence of a zero-sound mode. A table of predicted values for the zero polarization Fermi liquid parameters F_0^s and F_1^a is provided.

DOI: 10.1103/PhysRevB.85.224511 PACS number(s): 67.30.ep, 67.30.hr

I. INTRODUCTION

Thin ^{3}He films have been studied for many years as prototypical two-dimensional Fermi liquids.[1–6] Fermi liquid theory, developed by Landau[7] in the mid-1950s, showed how the low-temperature collective excitations and thermodynamic properties could be encoded in a few parameters, the Landau parameters, and that these parameters were related to a certain limiting value of the microscopic scattering function.[8]

In the 1970s, experiments on ^{3}He adsorbed onto exfoliated graphite stimulated theoretical work on Fermi liquid theory for two-dimensional systems.[9,10] In particular, Bloom[9] adapted Galitskii's approach[11] for the three-dimensional Fermi gas to the two-dimensional Fermi gas and evaluated the resulting principal value integrals numerically. In 1992, Engelbrecht, Randeria, and Zhang[12] (ERZ) obtained an analytic solution for the s-wave contribution to the low-density, unpolarized Fermi gas in two dimensions. The perturbation theory approach used by ERZ was applied to the low-density Fermi gas in three dimensions by Abrikosov and Khalatnikov (AK).[13] The exact solution by ERZ provided some corrections to the previous numerical results of Bloom. As stressed by ERZ the key to obtaining analytic results in two dimensions is the constant density of states.

In a recent paper[14] (AM) the perturbation theory approach of ERZ was generalized to include p-wave T-matrix interactions. The Landau parameters were calculated exactly and analytically to quadratic order in the interaction parameters. These Landau parameters can thus be used at arbitrarily high values of the polarization. A rigorous discussion of the generalization of Fermi liquid theory to polarized systems was given by Bedell and Quader.[15]

In this paper, we utilize the polarization-dependent results of AM and also include density dependence. We determine Landau parameters for both second-layer ^{3}He films on a graphite substrate and also submonolayer ^{3}He adsorbed in thin ^{4}He superfluid films. In Sec. II we very briefly describe the perturbation theory needed to compute the Landau parameters, and in Sec. III we review the expressions for the polarization-dependent effective masses, heat capacity, compressibility, spin susceptibility, zero-sound and spin-zero-sound collective excitations that were derived in AM. We also derive and discuss the conditions for thermodynamic stability in an arbitrarily polarized Fermi liquid film. In Sec. IV we discuss our results for second-layer ^{3}He films on graphite and in Sec. V we discuss our results for the adsorbed film mixtures. In order to compute the values of the s-wave and p-wave interaction components we fit existing measurements of the effective mass and spin susceptibility in these thin film systems. Section VI is the conclusion.

II. FERMI LIQUID THEORY

In this section, we very briefly review those results from Fermi liquid theory necessary to analyze the thermodynamics and collective excitations in thin ^{3}He films. For the details of the derivations of these expressions, please see AM.

A. Landau parameters

We examine a system of $N = N_\uparrow + N_\downarrow$, spin-$\frac{1}{2}$ fermions in a box of area L^2. The particles have bare mass m, and interact with two-body potential $V(r)$ that is assumed to depend only on the scalar distance between the particles. The particles fill two Fermi seas up to Fermi momenta $k_\uparrow$ and $k_\downarrow$, and we introduce the convention that the spin-down Fermi sea will always be the minority Fermi sea in the case of nonzero polarization. The term *polarization* denotes the magnetization per particle $M/N = (N_\uparrow - N_\downarrow)/N$. The terms coverage and areal density (N/L^2) are used interchangeably.

In second-order of perturbation theory, the ground-state energy can be written[16]

$$\begin{aligned} E = & \frac{1}{2}\sum_{\mathbf{p},\mathbf{q},\sigma}(V(0)-V(2p))\left(n_{\mathbf{p}+\frac{\mathbf{q}}{2},\sigma}\, n_{-\mathbf{p}+\frac{\mathbf{q}}{2},\sigma}\right) \\ & + \frac{1}{2}\sum_{\mathbf{p},\mathbf{q}} V(0)\left(n_{\mathbf{p}+\frac{\mathbf{q}}{2},\uparrow}\, n_{-\mathbf{p}+\frac{\mathbf{q}}{2},\downarrow} + n_{\mathbf{p}+\frac{\mathbf{q}}{2},\downarrow}\, n_{-\mathbf{p}+\frac{\mathbf{q}}{2},\uparrow}\right) \\ & + \frac{1}{2}\sum_{\mathbf{p},\mathbf{p}',\mathbf{q},\sigma}\frac{|V(\mathbf{p}-\mathbf{p}')|^2 - V(\mathbf{p}-\mathbf{p}')V(-\mathbf{p}-\mathbf{p}')}{\Delta T} \\ & \times\left(n_{\mathbf{p}+\frac{\mathbf{q}}{2},\sigma}\, n_{-\mathbf{p}+\frac{\mathbf{q}}{2},\sigma}\left(1-n_{\mathbf{p}'+\frac{\mathbf{q}}{2},\sigma}\right)\left(1-n_{-\mathbf{p}'+\frac{\mathbf{q}}{2},\sigma}\right)\right) \\ & + \sum_{\mathbf{p},\mathbf{p}',\mathbf{q}}\frac{|V(\mathbf{p}-\mathbf{p}')|^2}{\Delta T}\left(n_{\mathbf{p}+\frac{\mathbf{q}}{2},\uparrow}\, n_{-\mathbf{p}+\frac{\mathbf{q}}{2},\downarrow}\left(1-n_{\mathbf{p}'+\frac{\mathbf{q}}{2},\uparrow}\right)\right. \\ & \left.\times\left(1-n_{-\mathbf{p}'+\frac{\mathbf{q}}{2},\downarrow}\right)\right), \end{aligned} \tag{2.1}$$

where the kinetic energy denominators are given by

$$\Delta T = \frac{\hbar^2}{m}(p^2 - p'^2). \tag{2.2}$$

The spin variable $\sigma = \uparrow,\downarrow$ and the $n_{k,\sigma}$ are the noninteracting distribution functions, equal to 1 for $k < k_\sigma$ and 0 for $k > k_\sigma$. The potential function $V(p)$ is the Fourier transform of some local two-body interaction $V(r)$ as defined by the box normalized form:

$$V(p) = \frac{1}{L^2}\int d\mathbf{r} V(r) e^{i\mathbf{p}\cdot\mathbf{r}}. \tag{2.3}$$

It is important to note that $V(r)$ is an appropriately defined effective interaction and is not the very strong, bare ^{3}He-^{3}He interaction. For discussions pertaining to the construction of an effective interaction within the correlated basis functions approach, see Refs. 17 and 18.

Using the notation of Randeria, Duan, and Shieh,[19] $\langle \mathbf{k}\,|V|\,\mathbf{m}\rangle \equiv V(\mathbf{k}-\mathbf{m})$, the momentum matrix element can be written

$$\langle \mathbf{k}\,|V|\,\mathbf{m}\rangle = \sum_{\ell=0}^{\infty}\alpha_\ell T_\ell(\cos\theta_{km}) V_{km}^{(\ell)}, \tag{2.4}$$

where $\theta_{km} = \theta_{\mathbf{k}} - \theta_{\mathbf{m}}$, and we have defined

$$V_{km}^{(\ell)} = \frac{2\pi}{L^2}\int_0^\infty dr\, r J_\ell(kr) V(r) J_\ell(mr), \tag{2.5a}$$

the J_ℓ's are integer order Bessel functions, and

$$\alpha_\ell = \begin{cases} 1 & \text{if } \ell = 0, \\ 2 & \text{if } \ell \geqslant 1. \end{cases} \tag{2.5b}$$

The functions $T_\ell(\cos\theta) \equiv \cos(\ell\theta)$ are Chebyshev polynomials of the first kind.[20] They play the same role for angular variables in two dimensions that Legendre polynomials play in three dimensions.

The low-density theory is obtained by truncating the series Eq. (2.4) after the $\ell = 1$ term and then taking the low-density limits $kr \ll 1$ in the Bessel functions:

$$V(\mathbf{k}-\mathbf{m}) \approx V_0 + 2\cos(\theta_{km}) km V_1, \tag{2.6}$$

where the s-wave and p-wave low-density potential parameters are defined by

$$\begin{aligned} \lim_{k,m\to 0} V_{km}^{(0)} &\equiv V_0 = \frac{2\pi}{L^2}\int_0^\infty dr\, r V(r), \\ \lim_{k,m\to 0} V_{km}^{(1)} &\equiv km V_1 = \frac{km}{4}\frac{2\pi}{L^2}\int_0^\infty dr\, r^3 V(r). \end{aligned} \tag{2.7}$$

Thus, we find

$$V(\pm\mathbf{p}-\mathbf{p}') = V_0 \pm 2\cos(\theta_{pp'}) pp' V_1. \tag{2.8}$$

If one substitutes Eq. (2.8) into the energy Eq. (2.1) then one immediately finds divergences in the terms that are quadratic in the distribution functions. This was noticed by AK in three dimensions and was discussed in detail by ERZ for two dimensions. The divergences can be removed by replacing the bare interaction by an effective interaction, the two-particle T matrix.

Introducing an angular decomposition of the T-matrix Lippman-Schwinger equation yields

$$T_{pp'}^{(\ell)} = V_{pp'}^{(\ell)} + L^2\int_0^\infty \frac{dk}{2\pi} k V_{pk}^{(\ell)}\left(\frac{1}{E - 2\epsilon_k^0 + i\eta}\right) T_{kp'}^{(\ell)}, \tag{2.9}$$

where $\epsilon_k^0 \equiv \hbar^2 k^2/2m$. Inverting the low-density $\ell = 0,1$ equations and then truncating to second order in the T-matrix components yields

$$V_0 = \tau_0\,(1 - \mathbb{P}_0\tau_0)\,, \tag{2.10a}$$

$$V_1 = \tau_1\,(1 - \mathbb{P}_1\tau_1)\,, \tag{2.10b}$$

where, τ_0 and τ_1 are the low-energy limits of the T matrices,

$$\lim_{E\to 0} T_{pp'}^{(0)} = \tau_0, \tag{2.11a}$$

$$\lim_{E\to 0} T_{pp'}^{(1)} = pp'\tau_1, \tag{2.11b}$$

and $\mathbb{P}_0$ and $\mathbb{P}_1$ are integrals over the propagators that are used to cancel the divergences. For the details of the argument, see AM.

The Landau parameters $f_{k\,k'}^{\sigma\,\sigma'}$ are defined by

$$f_{k\,k'}^{\sigma\,\sigma'} = \frac{\delta^2 E}{\delta n_{k,\sigma}\delta n_{k',\sigma'}}. \tag{2.12}$$

Taking the functional derivatives and using symmetry arguments to simplify the expressions, we find

$$\begin{aligned} f_{k\,k'}^{\uparrow\uparrow} = & 4\sin^2(\theta_{k,k'}/2)k_\uparrow^2\tau_1 - 16\frac{m}{\hbar^2}\sum_{\mathbf{p},\mathbf{p}',\mathbf{q}}\frac{(pp'\cos(\theta_{pp'}))^2\tau_1^2}{p^2-p'^2}\left[\delta_{\mathbf{p}+\frac{\mathbf{q}}{2},\mathbf{k}'}\delta_{-\mathbf{p}+\frac{\mathbf{q}}{2},\mathbf{k}} n_{\mathbf{p}'+\frac{\mathbf{q}}{2},\uparrow} + 2\delta_{\mathbf{p}+\frac{\mathbf{q}}{2},\mathbf{k}'}\delta_{\mathbf{p}'+\frac{\mathbf{q}}{2},\mathbf{k}} n_{-\mathbf{p}+\frac{\mathbf{q}}{2},\uparrow}\right] \\ & - \frac{2m}{\hbar^2}\sum_{\mathbf{p},\mathbf{p}',\mathbf{q}}\frac{\tau_0^2 + 4pp'\cos(\theta_{pp'})\tau_0\tau_1 + 4(pp'\cos(\theta_{pp'}))^2\tau_1^2}{p^2-p'^2}\left[\delta_{\mathbf{p}+\frac{\mathbf{q}}{2},\mathbf{k}'}\delta_{\mathbf{p}'+\frac{\mathbf{q}}{2},\mathbf{k}} n_{-\mathbf{p}+\frac{\mathbf{q}}{2},\downarrow}\right]. \end{aligned} \tag{2.13}$$

The Landau parameter $f^{\downarrow\downarrow}_{kk'}$ is obtained from Eq. (2.13) by reversing all the spins. We note again that in the following, as a matter of convention, we will consider the spin-down Fermi sea as the minority Fermi sea when the polarization is nonzero. Finally, we have

$$f^{\uparrow\downarrow}_{kk'} = \tau_0 + \frac{1}{2}(\mathbf{k}-\mathbf{k}')^2\tau_1 - \frac{m}{\hbar^2}\sum_{\mathbf{p},\mathbf{p}',\mathbf{q}} \frac{\tau_0^2 + 4pp'\cos(\theta_{pp'})\tau_0\tau_1 + 4(pp'\cos(\theta_{pp'}))^2\tau_1^2}{p^2 - p'^2}$$
$$\times\left[\delta_{\mathbf{p}'+\frac{\mathbf{q}}{2},\mathbf{k}}\delta_{-\mathbf{p}+\frac{\mathbf{q}}{2},\mathbf{k}'}n_{\mathbf{p}+\frac{\mathbf{q}}{2},\uparrow} + \delta_{\mathbf{p}+\frac{\mathbf{q}}{2},\mathbf{k}}\delta_{-\mathbf{p}+\frac{\mathbf{q}}{2},\mathbf{k}'}n_{\mathbf{p}'+\frac{\mathbf{q}}{2},\uparrow} + \delta_{\mathbf{p}+\frac{\mathbf{q}}{2},\mathbf{k}}\delta_{-\mathbf{p}'+\frac{\mathbf{q}}{2},\mathbf{k}'}n_{-\mathbf{p}+\frac{\mathbf{q}}{2},\downarrow} + \delta_{\mathbf{p}+\frac{\mathbf{q}}{2},\mathbf{k}}\delta_{-\mathbf{p}+\frac{\mathbf{q}}{2},\mathbf{k}'}n_{-\mathbf{p}'+\frac{\mathbf{q}}{2},\downarrow}\right]. \quad (2.14)$$

The details of the integrations needed to evaluate Eqs. (2.13) and (2.14) can be found in AM. It is customary to use dimensionless forms for the parameters by multiplying the $f^{\sigma\sigma'}_{kk'}$'s by a density of states. [7] In the following we denote these dimensionless parameters by $\tilde{F}$, that is, $\tilde{F}^{\sigma\sigma'}_{kk'} = \tilde{N}_0 f^{\sigma\sigma'}_{kk'}$, where $\tilde{N}_0 = mL^2/2\pi\hbar^2$ is the *bare* single spin-state density of states. We introduce this tilde notation because it is customary to use an actual density of states in this definition. Our dimensionless Landau parameters thus differ from those introduced in Ref. 12 by the use of the bare mass instead of the effective mass and also by a factor of two. This choice is simply a matter of notational convenience and no physics depends on it. We also use the $\tilde{N}_0$'s to redefine the T-matrix parameters, τ_0 and τ_1:

$$g_0 = \tilde{N}_0\tau_0, \quad (2.15a)$$
$$g_1 = \tilde{N}_0\tau_1. \quad (2.15b)$$

We note that with this definition, g_0 is dimensionless, whereas g_1 has the dimensions of length squared.

The final results for the Landau parameters are

$$\tilde{F}^{\uparrow\uparrow}_{kk'} = 4k_\uparrow^2\sin^2\left(\frac{\theta_{kk'}}{2}\right)g_1 + \left[1 - \sqrt{1 - \frac{k_\downarrow^2}{k_\uparrow^2\sin^2\left(\frac{\theta_{kk'}}{2}\right)}}\,\Theta\left(k_\uparrow^2\sin^2\left(\frac{\theta_{kk'}}{2}\right) \geqslant k_\downarrow^2\right)\right]g_0^2 + \left[\left(\left(1 - \frac{16}{3}\sin^2\left(\frac{\theta_{kk'}}{2}\right)\right)k_\uparrow^2 + k_\downarrow^2\right)\right.$$
$$\left. - \sqrt{1 - \frac{k_\downarrow^2}{k_\uparrow^2\sin^2\left(\frac{\theta_{kk'}}{2}\right)}}\left(\left(1 - \frac{20}{3}\sin^2\left(\frac{\theta_{kk'}}{2}\right)\right)k_\uparrow^2 - \frac{1}{3}k_\downarrow^2\right)\Theta\left(k_\uparrow^2\sin^2\left(\frac{\theta_{kk'}}{2}\right) \geqslant k_\downarrow^2\right)\right]g_0g_1$$
$$+\left[\left(25 - 108\sin^2\left(\frac{\theta_{kk'}}{2}\right) + \frac{2240}{15}\sin^4\left(\frac{\theta_{kk'}}{2}\right)\right)\frac{k_\uparrow^4}{4} + \frac{k_\downarrow^4}{4} + \left(1 - 3\sin^2\left(\frac{\theta_{kk'}}{2}\right)\right)k_\uparrow^2k_\downarrow^2\right.$$
$$\left. - \sqrt{1 - \frac{k_\downarrow^2}{k_\uparrow^2\sin^2\left(\frac{\theta_{kk'}}{2}\right)}}\left[\left(1 - 12\sin^2\left(\frac{\theta_{kk'}}{2}\right) + \frac{448}{15}\sin^4\left(\frac{\theta_{kk'}}{2}\right)\right)\frac{k_\uparrow^4}{4} + \frac{k_\downarrow^4}{20} + \left(\frac{1}{2} - \frac{19}{15}\sin^2\left(\frac{\theta_{kk'}}{2}\right)\right)k_\uparrow^2k_\downarrow^2\right]\right.$$
$$\left.\times\,\Theta\left(k_\uparrow^2\sin^2\left(\frac{\theta_{kk'}}{2}\right) \geqslant k_\downarrow^2\right) + k_\uparrow^4\tan^2\left(\frac{\theta_{kk'}}{2}\right)\left\{(1 + 2\cos\theta_{kk'}) - \left[\cos\theta_{kk'} + \sin^2\theta_{kk'}\ln\left(\tan\left(\frac{\theta_{kk'}}{2}\right)\right)\right]\right\}\right]g_1^2 \quad (2.16)$$

The quantities $\Theta(x)$ are generalized step functions and are defined such that $\Theta(x) = 1$ if x is true, and 0 if x is not true.

In the limit of zero polarization, we simply have $\tilde{F}^{\downarrow\downarrow}_{kk'} = \tilde{F}^{\uparrow\uparrow}_{kk'}$ and $\tilde{F}^{\downarrow\downarrow}_{kk'}$ is obtained from (2.16) by reversing all the spins. In the following, we assume finite polarization and $k_\downarrow < k_\uparrow$:

$$\tilde{F}^{\downarrow\downarrow}_{kk'} = 4k_\downarrow^2\sin^2\left(\frac{\theta_{kk'}}{2}\right)g_1 + g_0^2 + \left[\left(1 - \frac{16}{3}\sin^2\left(\frac{\theta_{kk'}}{2}\right)\right)k_\downarrow^2 + k_\uparrow^2\right]g_0g_1$$
$$+\left[\left(25 - 108\sin^2\left(\frac{\theta_{kk'}}{2}\right) + \frac{2240}{15}\sin^4\left(\frac{\theta_{kk'}}{2}\right)\right)\frac{k_\downarrow^4}{4} + \frac{k_\uparrow^4}{4} + \left(1 - 3\sin^2\left(\frac{\theta_{kk'}}{2}\right)\right)k_\downarrow^2k_\uparrow^2\right.$$
$$\left. + k_\downarrow^4\tan^2\left(\frac{\theta_{kk'}}{2}\right)\left\{(1 + 2\cos\theta_{kk'}) - \left[\cos\theta_{kk'} + \sin^2\theta_{kk'}\ln\left(\tan\left(\frac{\theta_{kk'}}{2}\right)\right)\right]\right\}\right]g_1^2. \quad (2.17)$$

$$\tilde{F}^{\uparrow\downarrow}_{kk'} = g_0 + \frac{1}{2}|\vec{k} - \vec{k'}|^2g_1 + \left[\left(\frac{k_\uparrow^2 - k_\uparrow k_\downarrow\cos\theta_{kk'}}{|\mathbf{k}-\mathbf{k}'|^2}\right) + \left(\frac{k_\downarrow^2 - k_\downarrow k_\uparrow\cos\theta_{kk'}}{|\mathbf{k}-\mathbf{k}'|^2}\right) - \ln\left(\frac{2p}{q}\right)\right]g_0^2$$
$$+\left[-\left(\frac{2p}{q}\right)\cos\theta_{pq}(k_\uparrow^2 - k_\downarrow^2) + (k_\uparrow^2 - k_\uparrow k_\downarrow\cos\theta_{kk'})\left[1 - \frac{8}{3}\frac{(k_\uparrow^2 - k_\uparrow k_\downarrow\cos\theta_{kk'})^2}{|\vec{k} - \vec{k'}|^4}\right]\right.$$
$$\left. + \frac{(k_\downarrow^2 - k_\downarrow k_\uparrow\cos\theta_{kk'})}{|\vec{k} - \vec{k'}|^2}\left(k_\downarrow^2 + (k_\uparrow^2 - 2k_\uparrow k_\downarrow\cos\theta_{kk'}) - \frac{8}{3}\frac{(k_\downarrow^2 - k_\downarrow k_\uparrow\cos\theta_{kk'})^2}{|\vec{k} - \vec{k'}|^2}\right)\right]g_0g_1$$

$$+\left[\frac{(k_\uparrow^2-k_\uparrow k_\downarrow\cos\theta_{kk'})}{|\overrightarrow{k}-\overrightarrow{k'}|^2}\frac{k_\uparrow^2}{2}\left[(k_\downarrow^2-2k_\uparrow k_\downarrow\cos\theta_{kk'})-\frac{k_\uparrow^2}{|\overrightarrow{k}-\overrightarrow{k'}|^2}(k_\uparrow^2-2k_\uparrow k_\downarrow\cos\theta_{kk'}+k_\downarrow^2\cos 2\theta_{kk'})-\frac{k_\uparrow^2}{2}\right]\right.$$
$$+\frac{(k_\downarrow^2-k_\uparrow k_\downarrow\cos\theta_{kk'})}{|\overrightarrow{k}-\overrightarrow{k'}|^2}\frac{k_\downarrow^2}{2}\left[(k_\uparrow^2-2k_\uparrow k_\downarrow\cos\theta_{kk'})-\frac{k_\downarrow^2}{|\overrightarrow{k}-\overrightarrow{k'}|^2}(k_\downarrow^2-2k_\uparrow k_\downarrow\cos\theta_{kk'}+k_\uparrow^2\cos 2\theta_{kk'})-\frac{k_\downarrow^2}{2}\right]$$
$$+\frac{\frac{1}{4}[(k_\uparrow^2-k_\uparrow k_\downarrow\cos\theta_{kk'})(k_\downarrow^2-2k_\uparrow k_\downarrow\cos\theta_{kk'})^2]+\frac{1}{4}[(k_\downarrow^2-k_\uparrow k_\downarrow\cos\theta_{kk'})(k_\uparrow^2-2k_\uparrow k_\downarrow\cos\theta_{kk'})^2]}{|\overrightarrow{k}-\overrightarrow{k'}|^2}$$
$$+\left[(k_\uparrow^2-k_\uparrow k_\downarrow\cos\theta_{kk'})^3\left[-\frac{4}{3}(k_\downarrow^2-2k_\uparrow k_\downarrow\cos\theta_{kk'})+\frac{k_\uparrow^2}{|\overrightarrow{k}-\overrightarrow{k'}|^2}\left(k_\uparrow^2-2k_\uparrow k_\downarrow\cos\theta_{kk'}+k_\downarrow^2\left(\cos 2\theta_{kk'}+\frac{2}{3}\sin^2\theta_{kk'}\right)\right)\right]\right.$$
$$\left.+(k_\downarrow^2-k_\uparrow k_\downarrow\cos\theta_{kk'})^3\left[-\frac{4}{3}(k_\uparrow^2-2k_\uparrow k_\downarrow\cos\theta_{kk'})+\frac{k_\downarrow^2}{|\overrightarrow{k}-\overrightarrow{k'}|^2}\left(k_\downarrow^2-2k_\uparrow k_\downarrow\cos\theta_{kk'}+k_\uparrow^2\left(\cos 2\theta_{kk'}+\frac{2}{3}\sin^2\theta_{kk'}\right)\right)\right]\right]$$
$$\times\frac{1}{|\overrightarrow{k}-\overrightarrow{k'}|^4}+\frac{4}{5}\frac{(k_\uparrow^2-k_\uparrow k_\downarrow\cos\theta_{kk'})^5+(k_\downarrow^2-k_\uparrow k_\downarrow\cos\theta_{kk'})^5}{|\overrightarrow{k}-\overrightarrow{k'}|^6}$$
$$-\left(\frac{4p^2}{q^2}\right)\cos(2\theta_{\mathrm{p,q}})\left(\frac{1}{4}(k_\uparrow^4+k_\downarrow^4\right)+\left(-p^2+\frac{q^2}{4}\right)\frac{1}{2}(k_\uparrow^2+k_\downarrow^2)\right)+\left[4p^2\cos^2(\theta_{pq})\frac{1}{2}(k_\uparrow^2+k_\downarrow^2)\right.$$
$$\left.\left.+\left(-p^2+\frac{q^2}{4}\right)\frac{p^2}{2}\left(1+\frac{4p^2}{q^2}\right)\cos(2\theta_{pq})-(2p^4)\ln\left(\frac{2p}{q}\right)\right]\right]g_1^2, \tag{2.18}$$

where $|\overrightarrow{k}-\overrightarrow{k'}|^2=(k_\uparrow^2+k_\downarrow^2-2k_\uparrow k_\downarrow\cos\theta_{kk'})$,$2\overrightarrow{p}=\overrightarrow{k}-\overrightarrow{k'}$,$\overrightarrow{q}=\overrightarrow{k}+\overrightarrow{k'}$.

We can now specialize these results to the unpolarized limit $\tilde{F}_{kk'}^{\sigma\sigma'}(0)$ with the magnetization $M/N=(N_\uparrow-N_\downarrow)/N=0$, and the fully polarized limit $\tilde{F}_{kk'}^{\sigma\sigma'}(1)$ with $M/N=1$. For the unpolarized limit, we set $k=k'=k_\mathrm{F}$,

$$\tilde{F}_{kk'}^{\uparrow\uparrow}(M/N=0)=\tilde{F}_{kk'}^{\downarrow\downarrow}(M/N=0)=4\sin^2\left(\frac{\theta_{kk'}}{2}\right)k_\mathrm{F}^2g_1+g_0^2+2\left(1-\frac{8}{3}\sin^2\left(\frac{\theta_{kk'}}{2}\right)\right)k_\mathrm{F}^2g_0g_1$$
$$+\left[\left(30-120\sin^2\left(\frac{\theta_{kk'}}{2}\right)+\frac{448}{3}\sin^4\left(\frac{\theta_{kk'}}{2}\right)\right)+4\tan^2\left(\frac{\theta_{kk'}}{2}\right)\left[(1+2\cos\theta_{kk'})\right.\right.$$
$$\left.\left.-\left(\cos\theta_{kk'}+\sin^2\theta_{kk'}\ln\left(\tan\left(\frac{\theta_{kk'}}{2}\right)\right)\right)\right]\right]\frac{k_\mathrm{F}^4}{4}g_1^2, \tag{2.19}$$

$$\tilde{F}_{kk'}^{\uparrow\downarrow}(M/N=0)=g_0+2\sin^2\left(\frac{\theta_{kk'}}{2}\right)k_\mathrm{F}^2g_1+\left(1-\ln\left(\frac{2p}{q}\right)\right)g_0^2+\frac{4}{3}\sin^2\left(\frac{\theta_{kk'}}{2}\right)k_\mathrm{F}^2g_0g_1+\left[8\left(\frac{2}{5}-\ln\left(\frac{2p}{q}\right)\right)\sin^4\left(\frac{\theta_{kk'}}{2}\right)\right.$$
$$\left.+2\tan^2\left(\frac{\theta_{kk'}}{2}\right)(1+2\cos\theta_{kk'})-2\cos\theta_{kk'}\sin^2\left(\frac{\theta_{kk'}}{2}\right)\left(1+\tan^2\left(\frac{\theta_{kk'}}{2}\right)\right)\right]\frac{k_\mathrm{F}^4}{4}g_1^2. \tag{2.20}$$

For the fully polarized limit, we set $k_\uparrow=k_\mathrm{F}$,$k_\downarrow=0$,

$$\tilde{F}_{kk'}^{\uparrow\uparrow}(M/N=1)=4\sin^2\left(\frac{\theta_{kk'}}{2}\right)k_\mathrm{F}^2g_1+\frac{4}{3}\sin^2\left(\frac{\theta_{kk'}}{2}\right)k_\mathrm{F}^2g_0g_1+\left[\left(6-24\sin^2\left(\frac{\theta_{kk'}}{2}\right)+\frac{448}{15}\sin^4\left(\frac{\theta_{kk'}}{2}\right)\right)\right.$$
$$\left.+\tan^2\left(\frac{\theta_{kk'}}{2}\right)(1+2\cos\theta_{kk'})-\tan^2\left(\frac{\theta_{kk'}}{2}\right)\left(\cos\theta_{kk'}+\sin^2\theta_{kk'}\ln\left(\tan\left(\frac{\theta_{kk'}}{2}\right)\right)\right)\right]k_\mathrm{F}^4g_1^2, \tag{2.21}$$

$$\tilde{F}_{kk'}^{\downarrow\downarrow}(M/N=1)=g_0^2+k_\mathrm{F}^2g_0g_1+\frac{1}{4}k_\mathrm{F}^4g_1^2, \tag{2.22}$$

$$\tilde{F}_{kk'}^{\uparrow\downarrow}(M/N=1)=g_0+\frac{1}{2}k_F^2g_1+g_0^2-\frac{8}{3}k_\mathrm{F}^2g_0g_1+\frac{26}{20}k_\mathrm{F}^4g_1^2. \tag{2.23}$$

III. THERMODYNAMICS AND COLLECTIVE EXCITATIONS

In this section, we present relations for the two-dimensional arbitrarily polarized Fermi system that connect the angular moments of the Landau parameters to measurable thermodynamic properties and collective excitations. Detailed derivations of the expressions can be found in AM. As shown by Landau[8] and Nozières and Luttinger[21] the Landau parameter $\tilde{F}_{\mathbf{p}\mathbf{p}'}^{\sigma\sigma'}$ is determined by the singular behavior of the scattering function with the momenta $\mathbf{p}$ and $\mathbf{p}'$ fixed at the Fermi momentum. Thus, the only degree of freedom is the angle between the

momenta. In two-dimensions the angular decomposition can be written

$$\tilde{F}^{\sigma\,\sigma'}_{\mathbf{p}\,\mathbf{p}'} = \sum_{\ell=0}^{\infty} \alpha_\ell \tilde{F}^{\sigma\,\sigma'}_{\ell} T_\ell(\cos\theta_{\mathbf{pp}'}), \tag{3.1}$$

where α_ℓ is the parameter defined in Eq. (2.5b), and $T_\ell(\cos\theta_{\mathbf{pp}'}) = \cos(\ell\theta_{\mathbf{pp}'})$ are the Chebyshev polynomials of the first kind introduced in the previous section. This form for the angular decomposition requires that $\tilde{F}(\theta)$ is periodic in θ with period 2π, that $\tilde{F}(\theta)$ is real, and that $\tilde{F}(\theta)$ is even in θ. Inverting the decomposition,

$$\tilde{F}^{\sigma\,\sigma'}_{m} = \frac{1}{\pi}\int_{-1}^{+1} dx\, w(x) \tilde{F}^{\sigma\,\sigma'}_{\mathbf{p}\,\mathbf{p}'} T_m(x), \tag{3.2}$$

where $w(x) = 1/\sqrt{1-x^2}$ is the integration weight. In obtaining Eq. (3.2) we have used the inner product of two Chebyshev polynomials [Eq. (3.3)]:

$$\int_{-1}^{+1} dx\, w(x) T_m(x) T_\ell(x) = \frac{\pi}{\alpha_m}\delta_{m,\ell}. \tag{3.3}$$

In general, when an integrand consists of powers of $\cos(\theta)$ times Chebyshev polynomials then integrals over θ from 0 to 2π can be changed to integrals over $\cos(\theta)$ from -1 to $+1$ multiplied by a factor of 2.

A. Thermodynamic quantities

The state-dependent effective mass for an arbitrarily polarized two-dimensional Fermi liquid is given by

$$\frac{m}{m^*_\sigma} = 1 - \left(\tilde{F}_1^{\sigma\,\sigma} + \frac{k_{\mathrm{F}-\sigma}}{k_{\mathrm{F}\sigma}}\tilde{F}_1^{\sigma\,-\sigma}\right). \tag{3.4}$$

In this expression the notation $-\sigma$ simply denotes the opposite of σ; thus, if $\sigma = \uparrow$ then $-\sigma = \downarrow$.

We can now obtain the effective masses in the unpolarized and fully polarized limits. For zero polarization, in agreement with ERZ, we obtain

$$\frac{m^*}{m} = \frac{1}{1-2\tilde{F}_1^s} = 1 + 2F_1^s, \tag{3.5}$$

where $F_1^s = (m^*/m)\tilde{F}_1^s \equiv N_0 f_1^s$ is a dimensionless Landau parameter written in terms of a single spin-state density of states that itself contains the effective mass. [Here and henceforth $N_0 \equiv m^* L^2/2\pi\hbar^2$ is used to denote the *single* spin-state density of states in the zero polarization case. In this paper all dimensionless Landau parameters are scaled by a single spin-state density of states.] The symmetric and antisymmetric Landau parameters used in the zero polarization limit are defined, as usual, by

$$\tilde{F}_\ell^{\sigma\,\sigma'} = \tilde{F}_\ell^s + \sigma\sigma'\tilde{F}_\ell^a, \tag{3.6}$$

where for this definition we associate $\sigma(\uparrow) = +1$, and $\sigma(\downarrow) = -1$. In the fully polarized limit ($k_\uparrow = k_{\mathrm{F}}, k_\downarrow = 0$):

$$\frac{m^*_\uparrow}{m} = \frac{1}{1-\tilde{F}_1^{\uparrow\uparrow}}, \tag{3.7a}$$

$$\frac{m^*_\downarrow}{m} = \frac{1}{1 - k_\uparrow \lim_{k_\downarrow\to 0}\left(\frac{\tilde{F}_1^{\uparrow\downarrow}}{k_\downarrow}\right)}. \tag{3.7b}$$

These results are similar to those in three-dimensions where they were discussed by Bedell.[22] Bedell argued from scattering theory that $\lim_{k_\downarrow\to 0}\tilde{F}_\ell^{\uparrow\downarrow} \to 0$ and $\lim_{k_\downarrow\to 0}\tilde{F}_\ell^{\downarrow\downarrow} \to 0$ for $\ell \geqslant 1$.

The low-temperature heat capacity is simply proportional to the number of available states. Thus, in a derivation that follows that in three dimensions,[23] we find

$$C = \frac{\pi^2}{3}\tilde{N}_0\left(\frac{m^*_\uparrow}{m} + \frac{m^*_\downarrow}{m}\right)k_{\mathrm{B}}^2 T = \frac{\pi k_{\mathrm{B}}^2 L^2}{6\hbar^2}\left(m^*_\uparrow + m^*_\downarrow\right)T. \tag{3.8}$$

The inverse isothermal compressibility is defined by

$$\kappa_T^{-1} = -A\left(\frac{\partial P}{\partial A}\right)_{T,N_\uparrow,N_\downarrow}. \tag{3.9}$$

In terms of the Landau parameters, we find for arbitrary polarization

$$\kappa_T^{-1} = \frac{2\pi\hbar^2}{m}\left[\left(\frac{m}{m^*_\uparrow} + \tilde{F}_0^{\uparrow\uparrow}\right)\overline{n}_\uparrow^2 + 2\tilde{F}_0^{\uparrow\downarrow}\overline{n}_\uparrow\overline{n}_\downarrow + \left(\frac{m}{m^*_\downarrow} + \tilde{F}_0^{\downarrow\downarrow}\right)\overline{n}_\downarrow^2\right]. \tag{3.10}$$

The compressibility is related to the first sound speed c_1 by $mc_1^2 = \kappa^{-1}/\overline{n}$. As pointed out by Landau, first sound does not propagate in fermion systems at absolute zero. The propagating mode, zero sound, is discussed in the next section. In the limit of zero polarization $\overline{n}_\uparrow = \overline{n}_\downarrow = \overline{n}/2$, and full polarization $\overline{n}_\uparrow = \overline{n}, \overline{n}_\downarrow = 0$, we find

$$\kappa_T^{-1}(0) = \frac{\pi\hbar^2}{m^*}\overline{n}^2\left[1 + 2\frac{m^*}{m}\tilde{F}_0^s\right] = \frac{\pi\hbar^2}{m^*}\overline{n}^2\left[1 + 2F_0^s\right], \tag{3.11a}$$

$$\kappa_T^{-1}(1) = \frac{2\pi\hbar^2}{m^*_\uparrow}\overline{n}^2\left[1 + \frac{m^*_\uparrow}{m}\tilde{F}_0^{\uparrow\uparrow}\right], \tag{3.11b}$$

where in Eqs. (3.10), (3.11a), and (3.11b) $\overline{n}_\sigma \equiv N_\sigma/A$ are areal densities.

The isothermal spin susceptibility is defined by

$$\chi = \frac{1}{A}\left(\frac{\partial M}{\partial h}\right)_{T,N}. \tag{3.12}$$

In terms of the Landau parameters, the spin susceptibility is given by

$$\chi^{-1} = \frac{\pi\hbar^2}{2m}\left[\left(\frac{m}{m^*_\uparrow} + \tilde{F}_0^{\uparrow\uparrow}\right) - 2\tilde{F}_0^{\uparrow\downarrow} + \left(\frac{m}{m^*_\downarrow} + \tilde{F}_0^{\downarrow\downarrow}\right)\right]. \tag{3.13}$$

For alternative derivations of the spin susceptibility, see Ref. 24. In the limit of zero and full polarization, we find

$$\chi^{-1}(0) = \frac{\pi\hbar^2}{m^*}\left[1 + 2\frac{m^*}{m}\tilde{F}_0^a\right] = \frac{\pi\hbar^2}{m^*}\left[1 + 2F_0^a\right], \tag{3.14a}$$

$$\chi^{-1}(1) = \frac{\pi\hbar^2}{2m}\left[\left(\frac{m}{m^*_\uparrow} + \tilde{F}_0^{\uparrow\uparrow}\right) - 2\tilde{F}_0^{\uparrow\downarrow} + \left(\frac{m}{m^*_\downarrow} + \tilde{F}_0^{\downarrow\downarrow}\right)\right]. \tag{3.14b}$$

B. Collective excitations

The derivation of the zero-sound dispersion relations proceeds as in three dimensions beginning with Landau's linearized kinetic equation:[23]

$$(s_\sigma - \cos\theta)u_{\mathbf{k}\sigma}(\theta) - \cos\theta \sum_{\sigma'} \frac{m^*_{\sigma'} L^2}{4\pi^2\hbar^2} \int_0^{2\pi} d\theta' f^{\sigma\sigma'}_{kk'} u_{\mathbf{k}'\sigma'}(\theta') = 0, \tag{3.15}$$

where $u_{\mathbf{k}\sigma}(\theta)$ is a Fermi-surface displacement function, $\mathbf{q}$ is the wave vector of the mode, θ is the angle between $\mathbf{k}$ and $\mathbf{q}$, θ' is the angle between $\mathbf{k}'$ and $\mathbf{q}$, and $s_\sigma \equiv \omega/q v_{\mathrm{F}\sigma}$ is the usual dimensionless frequency. Then after introducing angular decompositions we find

$$(s_\sigma - \cos\theta)\sum_{\ell=0}^{\infty} \alpha_\ell u_{\ell\sigma} T_\ell(\cos\theta) - \cos\theta \sum_{\sigma'} N_0^{\sigma'} \sum_{\ell=0}^{\infty} \alpha_\ell f_\ell^{\sigma\sigma'} u_{\ell\sigma'} T_\ell(\cos\theta) = 0. \tag{3.16}$$

There are two basic ways to analyze Eq. (3.16). The simpler approach, carried out in AM, is to truncate the series after $\ell = 2$, and then to compute moments by multiplying with $T_m(\cos\theta)$ and integrating over θ. We then find

$$c_{0\pm}^2 = \tfrac{1}{2}\left(A_{\uparrow\uparrow} v_{\mathrm{F}\uparrow}^2 + A_{\downarrow\downarrow} v_{\mathrm{F}\downarrow}^2\right) \pm \tfrac{1}{2}\sqrt{\left[A_{\uparrow\uparrow} v_{\mathrm{F}\uparrow}^2 + A_{\downarrow\downarrow} v_{\mathrm{F}\downarrow}^2\right]^2 - 4(A_{\uparrow\uparrow}A_{\downarrow\downarrow} - A_{\uparrow\downarrow}A_{\downarrow\uparrow}) v_{\mathrm{F}\uparrow}^2 v_{\mathrm{F}\downarrow}^2}. \tag{3.17}$$

The parameters are defined by

$$A_{\uparrow\uparrow} = \left(1 + \frac{1}{2}\frac{m^*_\uparrow}{m}\tilde{F}_0^{\uparrow\uparrow}\right)\left(1 + \frac{m^*_\uparrow}{m}\tilde{F}_1^{\uparrow\uparrow}\right) + \frac{1}{2}\frac{m^*_\uparrow m^*_\downarrow}{m^2}\tilde{F}_1^{\uparrow\downarrow}\tilde{F}_0^{\downarrow\uparrow}\frac{v_{\mathrm{F}\downarrow}}{v_{\mathrm{F}\uparrow}}, \tag{3.18a}$$

$$A_{\downarrow\downarrow} = \left(1 + \frac{1}{2}\frac{m^*_\downarrow}{m}\tilde{F}_0^{\downarrow\downarrow}\right)\left(1 + \frac{m^*_\downarrow}{m}\tilde{F}_1^{\downarrow\downarrow}\right) + \frac{1}{2}\frac{m^*_\downarrow m^*_\uparrow}{m^2}\tilde{F}_1^{\downarrow\uparrow}\tilde{F}_0^{\uparrow\downarrow}\frac{v_{\mathrm{F}\uparrow}}{v_{\mathrm{F}\downarrow}}, \tag{3.18b}$$

$$A_{\uparrow\downarrow} = \left(1 + \frac{1}{2}\frac{m^*_\downarrow}{m}\tilde{F}_0^{\downarrow\downarrow}\right)\frac{m^*_\downarrow}{m}\tilde{F}_1^{\uparrow\downarrow} + \frac{1}{2}\frac{m^*_\downarrow}{m}\tilde{F}_0^{\uparrow\downarrow}\left(1 + \frac{m^*_\uparrow}{m}\tilde{F}_1^{\uparrow\uparrow}\right)\frac{v_{\mathrm{F}\uparrow}}{v_{\mathrm{F}\downarrow}}, \tag{3.18c}$$

$$A_{\downarrow\uparrow} = \left(1 + \frac{1}{2}\frac{m^*_\uparrow}{m}\tilde{F}_0^{\uparrow\uparrow}\right)\frac{m^*_\uparrow}{m}\tilde{F}_1^{\downarrow\uparrow} + \frac{1}{2}\frac{m^*_\uparrow}{m}\tilde{F}_0^{\downarrow\uparrow}\left(1 + \frac{m^*_\downarrow}{m}\tilde{F}_1^{\downarrow\downarrow}\right)\frac{v_{\mathrm{F}\downarrow}}{v_{\mathrm{F}\uparrow}}. \tag{3.18d}$$

In the weak coupling limit $A_{\sigma\sigma'} = 1$ and thus $c_{0\sigma} = v_{\mathrm{F}\sigma}$. For convenience, in the following we refer to this approach as the truncated series method.

In the zero-polarization limit ($A_{\uparrow\uparrow} = A_{\downarrow\downarrow}$, $A_{\uparrow\downarrow} = A_{\downarrow\uparrow}$, $v_{\mathrm{F}} = v_{\mathrm{F}\uparrow} = v_{\mathrm{F}\downarrow}$), and $c_{0\pm}^2 = (A_{\uparrow\uparrow} \pm |A_{\uparrow\downarrow}|)v_{\mathrm{F}}^2$. In terms of the Landau parameters,

$$\frac{c_{0\,s,a}^2}{v_{\mathrm{F}}^2} = \left(1 + F_0^{s,a}\right)\left(1 + 2F_1^{s,a}\right), \tag{3.19}$$

where we changed $+$ and $-$ to symmetric and antisymmetric, respectively. The symmetric mode corresponds to zero sound and the antisymmetric mode corresponds to spin zero sound. In the "simplest approximation"[25] we set $F_1^{s,a} = 0$ and find

$$c_{0\,s,a}^2 \approx \left(1 + F_0^{s,a}\right) v_{\mathrm{F}}^2. \tag{3.20}$$

Thus, in the zero-polarization, strong coupling limit we find $\lim_{F_0^{s,a}\to\infty} c_{0\,s,a}/v_{\mathrm{F}} \approx \sqrt{F_0^{s,a}}$. In the limit of full polarization ($v_{\mathrm{F}} = v_{\mathrm{F}\uparrow}$ and $v_{\mathrm{F}\downarrow} = 0$), we immediately find $c_{0+}^2 = A_{\uparrow\uparrow} v_{\mathrm{F}}^2$ and $c_{0-}^2 = 0$. Thus, in terms of the Landau parameters

$$c_{0+}^2 = \left(1 + \frac{1}{2}\frac{m^*_\uparrow}{m}\tilde{F}_0^{\uparrow\uparrow}\right)\left(1 + \frac{m^*_\uparrow}{m}\tilde{F}_1^{\uparrow\uparrow}\right) v_{\mathrm{F}}^2. \tag{3.21}$$

For the second approach to analyze the kinetic equation we follow Khalatnikov and Abrikosov[26] (see also Refs. 7 and 23) and rewrite the kinetic equation,

$$u_{m\sigma} - \sum_{\sigma'} N_0^{\sigma'} \sum_{\ell=0}^{\infty} \alpha_\ell f_\ell^{\sigma\sigma'} u_{\ell\sigma'} \Omega^\sigma_{m,\ell} = 0, \tag{3.22}$$

where the angular integrals are defined by

$$\Omega^\sigma_{m,\ell} \equiv \frac{1}{\pi}\int_{-1}^{+1} dx\, w(x) T_m(x)\left(\frac{x}{s_\sigma - x}\right) T_\ell(x). \tag{3.23}$$

The integrals can be evaluated analytically and we find

$$2\Omega^\sigma_{m,\ell} = \frac{1 + z_0^2}{1 - z_0^2}\left(z_0^{m+\ell} + z_0^{|m-\ell|}\right) - \delta_{m,\ell} - \delta_{m,0}\delta_{\ell,0}, \tag{3.24}$$

where

$$z_0 \equiv z_0^\sigma = s_\sigma - \sqrt{s_\sigma^2 - 1}. \tag{3.25}$$

In the "simplest approximation" we ignore all terms except $m = 0$. Then the zero-sound velocity, in the zero-polarization limit for simplicity, is determined by the solution of $1 - 2F_0^s\Omega_{0,0} = 0$, where

$$\Omega_{0,0} = \frac{s}{\sqrt{s^2 - 1}} - 1. \tag{3.26}$$

Solving for the zero-sound velocity,

$$\frac{c_{0s}^2}{v_{\mathrm{F}}^2} = \frac{\left(1 + 2F_0^s\right)^2}{1 + 4F_0^s}. \tag{3.27}$$

The Khalatnikov/Abrikosov approach has the correct weak coupling limit, and in the *strong* coupling limit $c_s^2/v_F^2 \sim F_0^s$, it is in agreement with Eq. (3.20). In numerical work to be discussed below, we show that we need to include contributions up to $\ell = 3$ terms in the set of coupled equations, Eq. (3.22) to ensure accurate results. The zero-sound and spin-zero-sound speeds are then the real eigenvalues of an 8×8 determinant. We note that in the important range of values of $F_0^s \approx 1$, the zero-sound speeds calculated with Eq. (3.20) tend to be slightly higher than those calculated with Eq. (3.27).

It is customary to compare the zero-sound speed with the first sound speed. From Eq. (3.11a) the zero-polarization first sound speed is given by

$$\frac{c_1^2}{v_F^2} = \frac{1}{2}\left(1 + 2F_1^s\right)\left(1 + 2F_0^s\right). \tag{3.28}$$

Thus, in the strong coupling limit $c_1^2/v_F^2 \sim F_0^s$, and the zero-sound and first-sound speeds become equal, the same as in three dimensions. In the weak coupling limit $c_1^2/v_F^2 \sim 1/2$, and thus $c_1/c_0 \sim 1/\sqrt{2}$.

C. Thermodynamic stability

The onset of instability is signaled by a pole in the scattering amplitudes.[25] Expressions for the scattering amplitudes of an arbitrarily polarized two-dimensional Fermi liquid can be found in Eqs. (3.47) in AM. The denominator of the scattering amplitude is isomorphic to the zero-frequency linearized kinetic equation. Thus, the intimate connection between the divergence of the scattering amplitude and the appearance of a soft mode. The general stability relation can be written

$$\left(\frac{m}{m_\uparrow^*} + \tilde{F}_\ell^{\uparrow\uparrow}\right)\left(\frac{m}{m_\downarrow^*} + \tilde{F}_\ell^{\downarrow\downarrow}\right) \geqslant (\tilde{F}_\ell^{\uparrow\downarrow})^2. \tag{3.29}$$

The stable regime is the one where the inequality in Eq. (3.29) is obeyed. This can only be shown by analyzing the response functions and the thermodynamic potential.

For simplicity, we introduce an alternate notation:

$$a_\ell^\uparrow = \frac{m}{m_\uparrow^*} + \tilde{F}_\ell^{\uparrow\uparrow}, \tag{3.30a}$$

$$a_\ell^\downarrow = \frac{m}{m_\downarrow^*} + \tilde{F}_\ell^{\downarrow\downarrow}, \tag{3.30b}$$

$$b_\ell = \tilde{F}_\ell^{\uparrow\downarrow}. \tag{3.30c}$$

The inverse compressibility and the inverse spin susceptibility Eqs. (3.10) and (3.13), respectively, can be written

$$\kappa_T^{-1} = \frac{2\pi\hbar^2}{m}[a_0^\uparrow \overline{n}_\uparrow^2 + a_0^\downarrow \overline{n}_\downarrow^2 + 2b_0 \overline{n}_\uparrow \overline{n}_\downarrow], \tag{3.31}$$

$$\chi^{-1} = \frac{\pi\hbar^2}{2m}[a_0^\uparrow + a_0^\downarrow - 2b_0]. \tag{3.32}$$

We note that these expressions only involve the $\ell = 0$ Landau parameters. We can now apply the following inequality:

$$a_\ell^\uparrow + a_\ell^\downarrow \geqslant 2\sqrt{a_\ell^\uparrow a_\ell^\downarrow} = 2|b_\ell|. \tag{3.33}$$

The equal sign in Eq. (3.33) simply denotes the zero of the stability condition. By inspection we see that the response functions are positive when the stability inequality Eq. (3.29) $a_0^\uparrow a_0^\downarrow > b_0^2$ is satisfied. Further, the response functions pass through zero when $a_0^\uparrow a_0^\downarrow = b_0^2$, and finally they become negative when $a_0^\uparrow a_0^\downarrow < b_0^2$.

The general stability relation also ensures positive effective masses at the Fermi surface and thus positive heat capacities. If one takes the $\lim m_\uparrow^* \to 0^+$ say, the left-hand side of (3.29) becomes large and positive and the inequality is obeyed. However, when one passes through the pole then the left-hand side becomes large and negative and the inequality is not obeyed. From Eq. (3.4) we note that the condition for positive effective masses in terms of the Landau parameters can be written: $\tilde{F}_1^{\sigma\,\sigma} + (k_{F-\sigma}/k_{F\sigma})\tilde{F}_1^{\sigma\,-\sigma} < 1$. In the zero polarization limit this becomes $2F_1^s > -1$ where $F_1^s = (m^*/m)\tilde{F}_1^s$. We note that the expression for the effective mass Eq. (3.4) can be substituted into the general stability relation to derive an inequality for the $\ell = 1$ Landau parameters.

An alternate path to showing that the stable regime is defined by Eq. (3.29) is to follow Pomeranchuk[27] and expand the thermodynamic potential to second order in deformations of the Fermi surface $\delta p_{F\sigma}$. We can then show that the general stability relation determines the regime in which the thermodynamic potential is a minimum. We follow Baym and Pethick[23] to obtain for the second-order variation in the thermodynamic potential

$$\delta E - \mu\delta N = \sum_{\ell=0}^{\infty} \alpha_\ell \frac{1}{2}\tilde{N}_0[\eta_\uparrow^2 a_\ell^\uparrow + 2\eta_\uparrow\eta_\downarrow b_\ell + \eta_\downarrow^2 a_\ell^\downarrow], \tag{3.34}$$

where $\eta_\sigma = (m_\sigma^*/m)v_{\ell\sigma}$ and the $v_{\ell\sigma}$ are the expansion coefficients for the Fermi surface deformations:

$$v_{F\sigma}\delta p_{F\sigma} = \sum_{\ell=0}^{\infty} \alpha_\ell v_{\ell\sigma} T_\ell(\cos\theta). \tag{3.35}$$

The argument of the sum in Eq. (3.34) is in the same form as that of the inverse compressibility, and so we can conclude that the thermodynamic potential is a minimum when the general stability relation is obeyed.

IV. ^{3}He THIN FILMS ON GRAPHITE

We begin by determining values for the effective interaction parameters g_0 and g_1. We do this by fitting them to the experimental values of the effective mass and spin susceptibility as a function of density. The application of the low-density theory of Sec. II to films where the typical density is approximately one-half of a monolayer needs to be discussed. We need to emphasize that all that we are requiring of the low-density perturbation theory is that the functional form for the energy be a reasonable approximation at these moderate densities. The g_0 and g_1 that we find from this procedure are *not* the values one would calculate from first principles in the zero density limit. The fitted parameters clearly must include contributions from the higher ℓ states. Thus, we call them *effective* interaction parameters. We show *a posteriori* that the effective interaction parameters have only a very modest dependence on density.

For second-layer ^{3}He adsorbed on graphite, the spin susceptibility data can be obtained from Fig. 1 of Ref. 4, and the effective mass data can be obtained from Fig. 12 of Ref. 3.

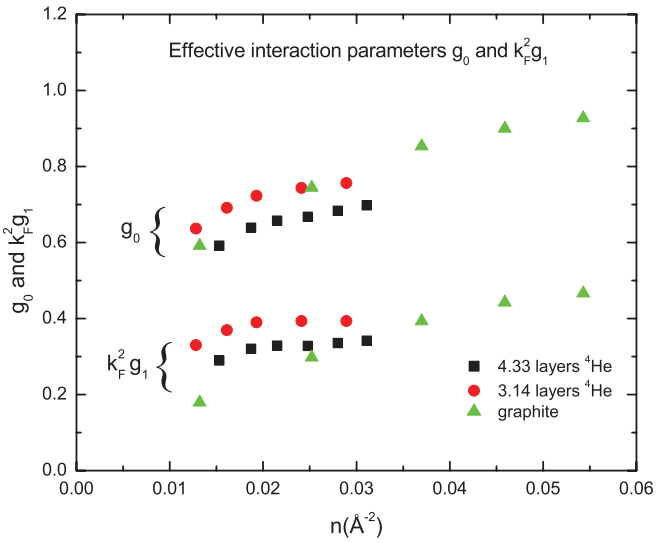

FIG. 1. (Color online) The fitted values of the effective interaction parameters g_0 and $k_F^2 g_1$ as a function of film coverage. The triangles are determined from measurements of the effective mass and spin susceptibility of second-layer ^{3}He on a graphite substrate from Refs. 3 and 4, respectively. The squares and circles are from ^{3}He-^{4}He thin mixture film data of Ref. 28.

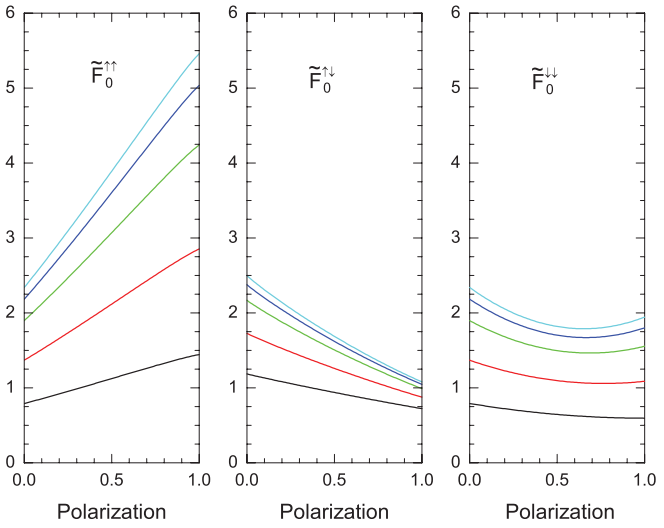

FIG. 2. (Color online) The Landau parameters $\tilde{F}_0^{\uparrow\uparrow}, \tilde{F}_0^{\uparrow\downarrow}$, and $\tilde{F}_0^{\downarrow\downarrow}$ for a thin ^{3}He film on graphite at five coverages as a function of polarization. In each figure the lowest curve corresponds to the lowest coverage, and the curves progress in order up to the highest curve at the highest coverage. The five coverages are $\overline{n} = 0.0132$, 0.0252, 0.0370, 0.0459, and 0.0543 Å^{-2}.

All experiments are done at small or zero polarization. The five densities at which results are reported in this section are $\overline{n} = 0.0132$, 0.0252, 0.0370, 0.0459, and 0.0543 Å^{-2}.

In Fig. 1 we show the values obtained for the effective interaction parameters as a function of ^{3}He density. In order to compare approximately the magnitudes of the s-wave and p-wave interaction components, we multiply g_1 by k_F^2 to create a dimensionless quantity. Then $g_1 k_F^2$ is the quantity displayed in Fig. 1. The effective interaction parameters for the second layer of ^{3}He on graphite data are shown as triangles. Both g_0 and $k_F^2 g_1$ increase monotonically as a function of coverage. Nevertheless, the density dependence is modest considering that the range of density from smallest to largest covers almost a factor of six. The squares and circles are from ^{3}He-^{4}He thin mixture film data Ref. 28 and are discussed in the next section.

With values for the s-wave and p-wave interaction components, we can follow the analysis in Sec. II and compute the Landau parameters $\{\tilde{F}^{\uparrow\uparrow}, \tilde{F}^{\uparrow\downarrow}, \tilde{F}^{\downarrow\downarrow}\}$ for a ^{3}He thin film. We then compute the components of an angular momentum decomposition of the Landau parameters which, from Sec. III, yield various measurable quantities.

Figures 2 and 3 show the $\ell = 0, 1$ angular components of the Landau parameters. The Landau parameter $\tilde{F}_0^{\uparrow\uparrow}$ increases monotonically with increasing density at fixed polarization, and also increases monotonically with increasing polarization at fixed density. At zero polarization, the $\tilde{F}_0^{\uparrow\downarrow}$ are similar in magnitude to $\tilde{F}_0^{\uparrow\uparrow}$ at a given density; however, they decrease monotonically with increasing polarization at a fixed density. The $\tilde{F}_0^{\downarrow\downarrow}$, as usual, increase with increasing density at a fixed polarization; however, they then pass through a minimum at around 70% polarization at the higher densities.

Figure 3 shows that the $\ell = 1$ parameters are almost all monotonically decreasing functions of polarization at a given density. The negative values of $\tilde{F}_1^{\uparrow\uparrow}$ at high polarizations drive the high-polarization values of $m_\uparrow^*/m$ to below 1, as is discussed below. At zero polarization the $\tilde{F}_1^{\uparrow\downarrow}$ parameter dominates, whereas at complete polarization the $\tilde{F}_1^{\uparrow\uparrow}$ has the greatest magnitude, as is to be expected. Further, at complete polarization $\tilde{F}_1^{\uparrow\downarrow} = \tilde{F}_1^{\downarrow\downarrow} = 0$, which ensures that the spin-down effective mass in that limit Eq. (3.7b) is well defined.

In order to examine the convergence of the angular expansion Fig. 4 shows the Landau parameters $\tilde{F}_\ell^{\uparrow\uparrow}$ as a function of ℓ for polarizations 0, 0.5, 1.0 at density $\overline{n} = 0.0132$ Å^{-2}. One of the advantages of fitting the effective interactions rather than

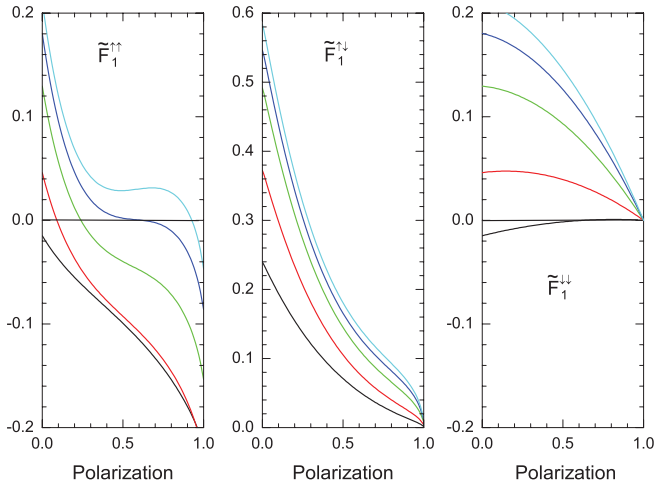

FIG. 3. (Color online) The Landau parameters $\tilde{F}_1^{\uparrow\uparrow}, \tilde{F}_1^{\uparrow\downarrow}$, and $\tilde{F}_1^{\downarrow\downarrow}$ for a thin ^{3}He film on graphite at five coverages as a function of polarization M/N. In each figure the lowest curve corresponds to the lowest coverage, and the curves progress in order up to the highest curve at the highest coverage. The five coverages are $\overline{n} = 0.0132$, 0.0252, 0.0370, 0.0459, and 0.0543 Å^{-2}.

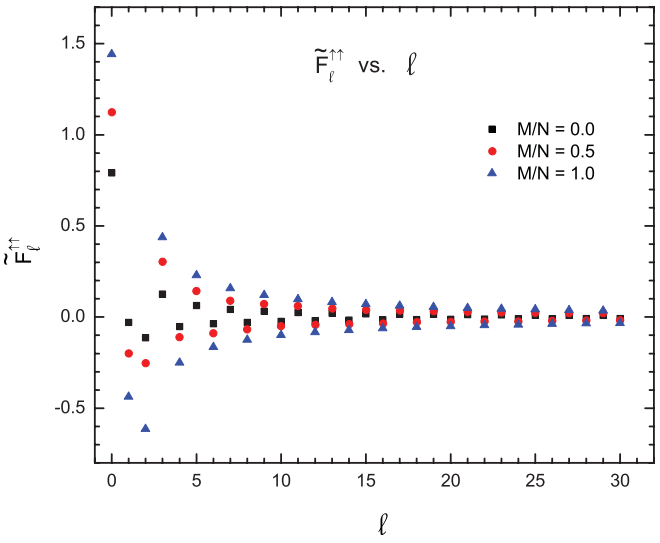

FIG. 4. (Color online) The Landau parameters $\tilde{F}_\ell^{\uparrow\uparrow}$ as a function of ℓ for ^{3}He on graphite at a coverage of $\overline{n} = 0.0132$ Å^{-2} for three polarizations: $M/N = 0$, 0.5, and 1.0. The series oscillates in sign for $\ell \geqslant 2$. Notice that the $\ell = 1$ terms and the $\ell = 2$ terms have the same sign. Further, the magnitude of the $\ell = 2$ terms are greater than the magnitudes of the $\ell = 1$ terms.

the Landau parameters directly is that we can readily compute Landau parameters for any value of ℓ. The magnitudes of the parameters certainly decrease as a function of ℓ. However, it is not clear that the angular decomposition could be considered as converged with only the $\ell = 0$ and $\ell = 1$ terms, as is sometimes assumed for the bulk ^{3}He system. In fact, the $\ell = 2$ terms have the same sign and a greater magnitude than $\ell = 1$ terms. It is because of this behavior that we investigate the importance of keeping components up to $\ell = 3$ in order to ensure accurate zero-sound speeds in the following section. For $\ell \geqslant 2$ the series oscillates in sign, with the signs for the odd terms positive and the signs for the even terms negative, and decreases uniformly in magnitude.

1. Thermodynamics

The expression for the effective mass as a function of polarization is given in Eq. (3.4). Using the $\ell = 1$ Landau parameters shown in Fig. 3 we calculate the results shown in Fig. 5. Both the spin-up and the spin-down effective masses are a maximum at zero polarization. They increase monotonically with increasing density at fixed polarization and decrease monotonically with increasing polarization at fixed density. At a fixed density and polarization, $m_\downarrow^* \geqslant m_\uparrow^*$. This behavior is in qualitative agreement with arguments presented by Bedell[15] for the three-dimensional system. The zero polarization value for the effective masses is one of the experimental numbers (from Ref. 3) used to determine the effective interaction components, g_0 and g_1. Thus, the behavior of m_σ^*/m as a function of polarization is one of the key predictions for this model. The distinguishing feature of these results is the dramatic decrease in the spin-up effective masses at the larger coverages as a function of polarization. Another interesting prediction of Fig. 5 is that $m_\uparrow^*$ falls below m at high polarization. From Eq. (3.7a) it is clear that this

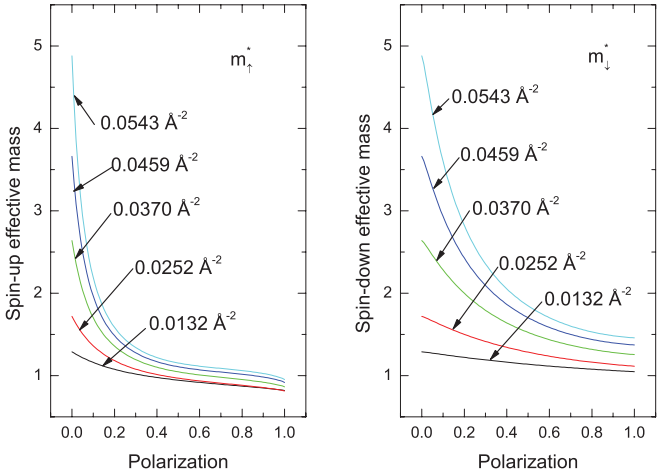

FIG. 5. (Color online) The spin-up and spin-down effective masses m_σ^*/m for a thin ^{3}He film on graphite as a function of polarization. The zero polarization limits are from Ref. 3, as discussed in the text.

behavior is being driven by $\tilde{F}_1^{\uparrow\uparrow}$ becoming negative at high polarization. Further, from Eq. (2.21) it is clear that in the limit $g_1 = 0$ we would have $m_\uparrow^* = m$ for the majority spin effective mass in the limit of 100% polarization.

The expression for the low-temperature heat capacity as a function of polarization is given in Eq. (3.8). In Fig. 6 we plot the slope of the specific heat. Since the number of accessible states gets smaller with increasing polarization, we expect that the heat capacity would decrease monotonically as a function of polarization and this is clearly shown in this figure. This behavior simply mirrors the decrease in the magnitude of the effective mass with increasing polarization.

In Fig. 7 we show the first sound speed c_1, essentially the inverse of the square root of the compressibility, as a function of polarization at five coverages. As pointed out by Landau [7] first sound cannot propagate in a Fermi liquid at absolute zero.

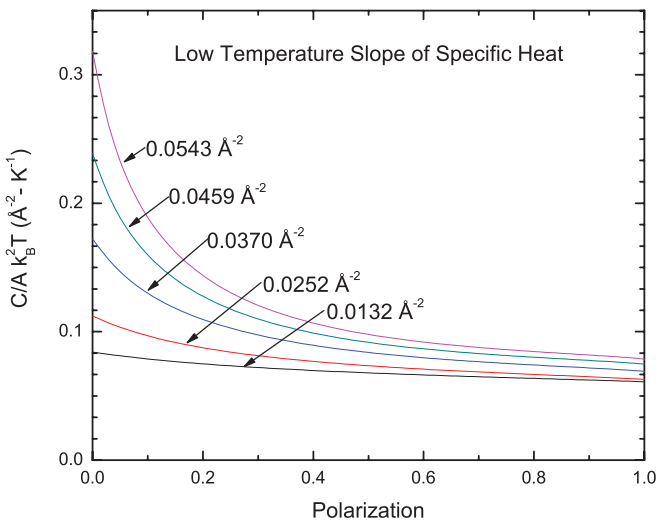

FIG. 6. (Color online) The slope of the low-temperature heat capacity for a thin ^{3}He film on graphite as a function of polarization. The slope decreases monotonically with increasing polarization, as expected from the behaviors of the state-dependent effective masses.

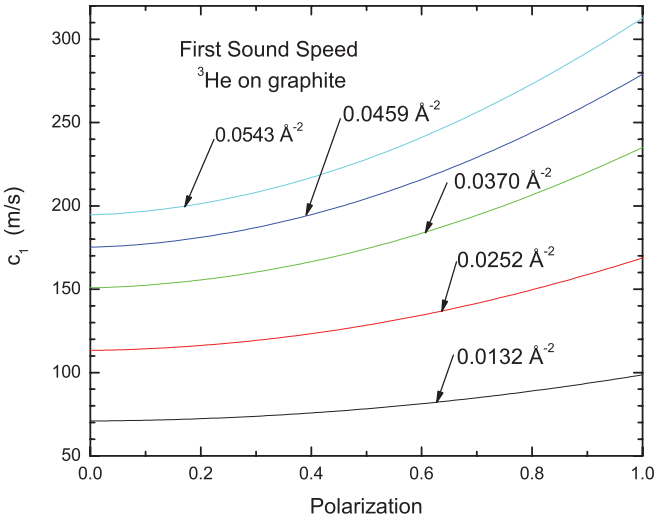

FIG. 7. (Color online) The speed of first sound for thin films of ^{3}He on graphite as a function of polarization shown for five coverages: $\overline{n} = 0.0132$, 0.0252, 0.0370, 0.0459, and 0.0543 Å^{-2}. Increasing magnitudes of first sound indicate that the system becomes less compressible with increasing polarization at fixed density.

At any finite temperature, however, hydrodynamic response will dominate in the limit of small frequencies.[29] As is expected the films become less compressible at fixed density with increasing polarization. Indirect information concerning the magnitude of c_1 can be obtained from the small-q behavior of the structure factor $S(q)$, as discussed in AM.

The inverse spin susceptibility Eq. (3.13) as a function of polarization for five ^{3}He coverages on graphite is shown in Fig. 8. The spin susceptibility is a monotonically decreasing function of the polarization at fixed coverage. Because the two-dimensional density of states $\tilde{N}_0$ is a constant the susceptibility does not vanish in the complete polarization limit as it does

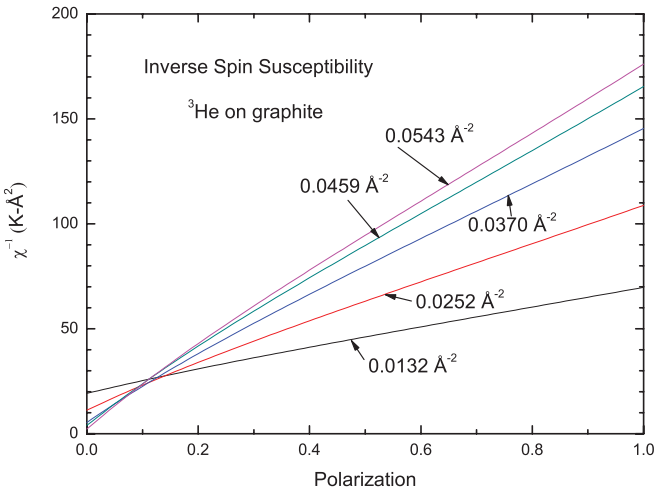

FIG. 8. (Color online) The inverse spin susceptibility for ^{3}He in two dimensions as a function of polarization at five densities as indicated by the labels in the figure. The densities are in units of Å^{-2}. We note that as a special feature of two dimensions the susceptibility does not vanish in the limit of complete polarization. The zero polarization limits are from Ref. 4, as discussed in the text.

in three dimensions. The density dependence is interesting. At low polarization, the largest spin susceptibility is at the lowest density. The susceptibilities seem to cross at a polarization $\approx$10%, and at large polarization, the largest spin susceptibility is at the largest density.

2. *Collective excitations*

The allowed collective modes at absolute zero in fermion systems correspond to oscillations of the Fermi seas and are known as zero sound. In Sec. III we derived two expressions for the zero-sound and spin-zero-sound speeds as a function of polarization. In the left panel of Fig. 9 we have plotted zero-sound speeds for both of the approximations at the smallest and largest areal densities that we are considering. In the figure we label the results of Eq. (3.17) "truncated series" and label the results of Eq. (3.22) "AK". Of course, each approach is just a different method of solving a truncated set of linear equations that result from Landau's kinetic equation. The AK approximation leads to lower zero-sound speeds at every polarization. The differences in the zero-sound eigenvalues between the two approaches is small, especially at the lowest density. There is an interesting crossing of the up-spin Fermi velocities at a polarization $\approx$10% that can be attributed to the polarization dependence of the effective masses. At finite polarization, the condition for stability of the collective excitation is that the speed be greater than the maximum Fermi velocity. In this system the maximum Fermi velocity is $v_{F\uparrow}$. By inspection of the left panel of Fig. 9 it is clear that zero sound will propagate at all polarizations for both densities.

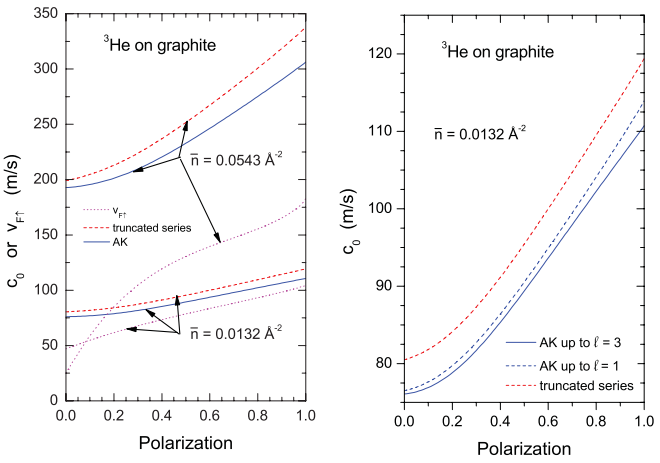

FIG. 9. (Color online) (Left) The zero-sound speed for ^{3}He on graphite at densities of $\overline{n} = 0.0132$ and 0.0543 Å^{-2} as a function of polarization. The solid lines are the AK results [Eq. (3.22)], the dotted lines are the "truncated series" results [Eq. (3.17)], and the dashed lines are the up-spin Fermi velocities, $v_{F\uparrow}$. These results imply that zero sound is stable over the whole range of polarizations and densities examined here. (Right) The zero-sound speed for ^{3}He on graphite at a density of $\overline{n} = 0.0132$ Å^{-2} as a function of polarization. The dotted line is the simple quadratic truncated series of Eq. (3.17), the dashed line is the AK approximation [Eq. (3.22)] truncated after $\ell = 1$, and the solid line is the AK approximation truncated after $\ell = 3$.

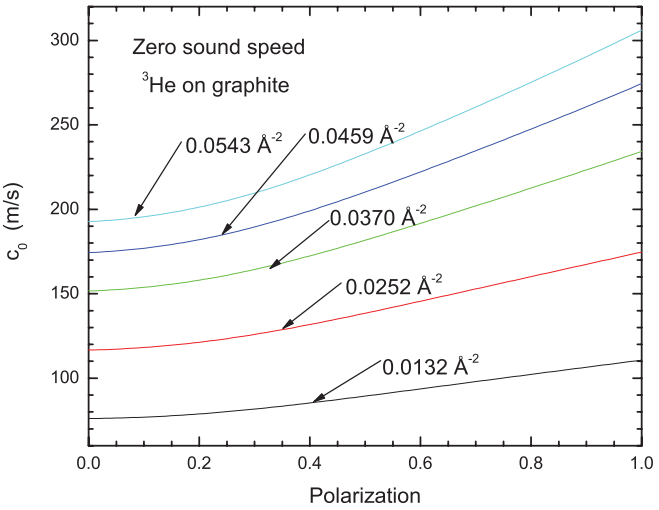

FIG. 10. (Color online) The zero-sound speeds as a function of polarization for second-layer ^{3}He on graphite. Each line is labeled by the coverage in units of Å^{-2}.

We have also addressed the question of convergence using the AK approximation. The results shown in the left panel of Fig. 9 were calculated after truncating the sets of coupled equations after the $\ell = 3$ contribution. This results in an 8×8 determinant to be diagonalized. In the right panel of Fig. 9 we examine the convergence by comparing the AK zero-sound speeds after truncating at $\ell = 1$ and $\ell = 3$, and we also show the truncated series results all at $\overline{n} = 0.0132$ Å^{-2}. The differences in the zero-sound speeds between the $\ell = 1$ truncation and the $\ell = 3$ truncation are only a few percent. Thus, we are confident that the results truncated after $\ell = 3$ are accurate. Then, in Fig. 10 we use the AK model including $\ell = 3$ terms as discussed above to calculate the zero-sound speeds for second layer ^{3}He on graphite as predicted by our model. Each line is labeled by the ^{3}He coverage in units of Å^{-2}.

3. *The zero-sound speeds*

We have not shown any results for spin zero sound because we do not find that this mode propagates. We do not find any density or polarization at which the antisymmetric spin mode speed has a magnitude greater than the spin-up Fermi velocity. We note that this corrects an error in Ref. 14, where in discussing the "truncated series" it was erroneously stated that for stability the spin-zero-sound mode only needs to be greater in magnitude than the Fermi velocity of the minority Fermi sea. Any mode with speed less than the maximum Fermi velocity will necessarily have a complex eigenvalue, as is clearly seen in the AK approach. Further, when one admits Landau parameters with $\ell > 1$ then the eigenvalue problem can, in principle, have multiple propagating zero-sound modes.[23] At every density and polarization examined for this work we find one and only one real, positive eigenvalue with magnitude greater than the maximum Fermi velocity. The nature of the mode is determined by examining the eigenfunctions.

Once we have obtained the angular moments of the Fermi surface distortion we can then build back the distortion as it

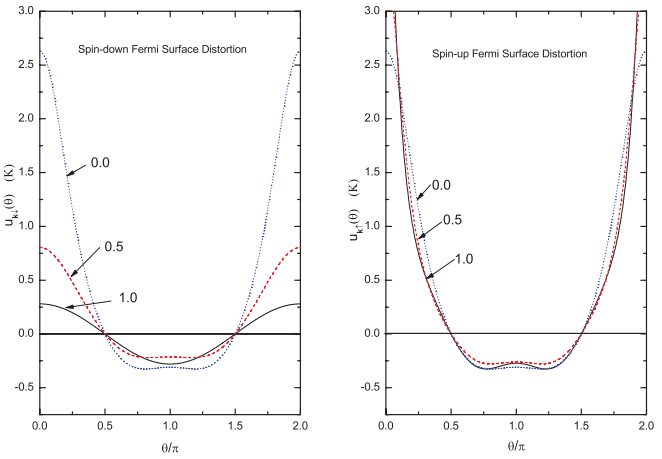

FIG. 11. (Color online) The spin-up and spin-down Fermi surface distortion $u_{\mathbf{k}\sigma}(\theta)$ for ^{3}He on graphite, at a density of $\overline{n} = 0.0132$ Å^{-2}, in units of degrees Kelvin. The distortion function is shown at three polarizations 0.0,0.5,1.0. In both Fermi seas the distortion corresponds to an elongation of the distribution in the direction of propagation of the excitation and a flattening out of the distribution in the opposite direction. The majority-spin Fermi sea distortion shows little polarization dependence, whereas the minority-spin Fermi sea distortion evolves to a cosine distribution in the limit of zero occupation as discussed in the text.

appears in momentum space:

$$u_{\mathbf{k}\sigma}(\theta) = \sum_{\ell=0}^{\infty} \alpha_\ell u_{\ell\sigma} T_\ell(\cos\theta), \tag{4.1}$$

In Fig. 11 we show the Fermi surface distortions for the up and down-spin Fermi seas at three polarizations: 0.0,0.5,1.0. There is little polarization dependence in the up-spin Fermi sea distortion. The excitation state changes the Fermi sea shape from a circle to conoidal with a large increase in the occupation of states in the direction of propagation and a flattening of the distribution in the opposite direction.

The form of the minority-spin surface distortion in the limit of complete polarization is interesting. The magnitude of the distortion in the forward direction for the spin-down Fermi sea decreases dramatically with increasing polarization. The distortion reaches a limiting cosine form as the polarization becomes complete. We examine Eq. (3.22) for $u_{\mathbf{k}\sigma}(\theta)$ in the $\lim k_{\mathrm{F}\downarrow} \to 0$. From Bedell's argument,[15] in the limit of complete polarization we have $f_\ell^{\uparrow\downarrow} = f_\ell^{\downarrow\downarrow} = 0$ for $\ell \geqslant 1$. Thus, in the complete polarization limit we only need examine $\Omega_{m\,0}^{\downarrow}$. By definition, in the complete polarization limit we also have $s_\downarrow \gg 1$ and thus from Eq. (3.25), $z_0 \approx 1/(2s_\downarrow)$. Substituting back into Eq. (3.24), we find that $\Omega_{10}^{\downarrow}$ is the leading term to $O(s_\downarrow^{-1})$ [note, $\Omega_{00}^{\downarrow} = O(s_\downarrow^{-2})$]. Reconstructing the surface deformation we find from Eq. (4.1) $\lim_{k_{\mathrm{F}\downarrow}\to 0} u_{k_{\mathrm{F}\downarrow}}(\theta) \approx 2u_1\cos(\theta)$. The cosine dependence is what is expected in a regime dominated by p-wave scattering.

V. ^{3}He IN THIN SUPERFLUID ^{4}He FILMS

The study of ^{3}He adsorbed in thin ^{4}He films was initiated by Gasparini and co-workers in the 1980s.[30] The substrate used by this group was Nuclepore, a polycarbonate material used

as filters in the life sciences. This group studied the energetics of the ^{3}He surface state using heat capacities as the probe. In Ref. 30 they reported evidence that the ^{3}He component may be condensing into a two-dimensional Fermi liquid as the temperature is lowered at fixed ^{3}He coverage. In the 1990s much of the work on ^{3}He-^{4}He thin mixture films was continued by Hallock and co-workers.[31] In particular, in Refs. 28, 32, and 33 they determined experimental values of the Landau parameters F_0^a and F_1^s for various coverages of ^{3}He and various ^{4}He film thicknesses.

The experimental results that we used for this analysis were taken from Fig. 6 in Ref. 28. To be specific, this figure shows values for the Landau parameters F_0^a and F_0^s as a function of ^{3}He areal density for two ^{4}He film thicknesses: 3.14 layers and 4.33 layers. We took those values, substituted them back into the expressions used by Akimoto, Cummings, and Hallock for the effective mass and spin susceptibility, and then we determined g_0 and g_1 from that data. The results of our analysis are shown in Fig. 1 by the disk-shaped (3.14 layers) and solid-square (4.33 layers) data points. The magnitudes of g_0 and $k_F^2 g_1$ for the 3.14-layer ^{4}He film are greater than those for the 4.33-layer film over the range of ^{3}He coverages that we examined. The graphite substrate effective interaction parameters are very similar to those of the thin-film mixture with perhaps a slight difference in slope. This similarity is reasonable since there are not large differences in the effective masses or spin susceptibilities for the two cases.

In Figs. 12 and 13 we show the $\ell = 0,1$ components of the Landau parameters for the 3.14-layer system. The functional forms of these Landau parameters are very similar to those in Figs. 2 and 3, as one would expect. The data for the mixture film extends over a smaller range of ^{3}He density than the graphite substrate data. For the mixture film the density range is roughly 0.01–0.03 Å^{-2}, whereas for the graphite the density range is 0.01–0.05 Å^{-2}. The difference is due to the onset of occupation of the first excited state in the mixture film at a density of ∼0.39 Å^{-2}.[34]

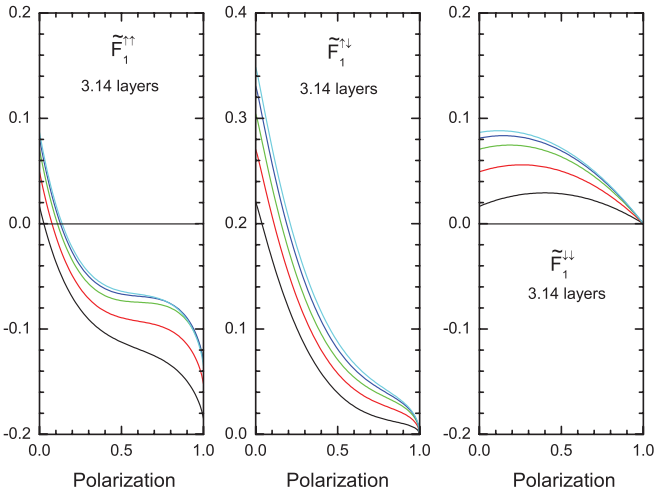

FIG. 13. (Color online) The Landau parameters $\tilde{F}_1^{\uparrow\uparrow}, \tilde{F}_1^{\uparrow\downarrow}$, and $\tilde{F}_1^{\downarrow\downarrow}$ for a thin ^{3}He film in a 3.14-layer ^{4}He film at five coverages as a function of polarization. In each figure the lowest curve corresponds to the lowest coverage, and the curves progress in order up to the highest curve at the highest coverage. The five coverages are $\overline{n} = 0.0128$, 0.0161, 0.0193, 0.0241, and 0.0289 Å^{-2}.

Figures 14 and 15 show the Landau parameters for the 4.33-layer film. As noted above, the effective interaction parameters for the 4.33-layer film are fairly uniformly spaced above the parameters for the 3.14-layer film (see Fig. 1). The Landau parameters are thus very similar in the two films but the 4.33-layer parameters are smaller in magnitude as a function of polarization.

In Fig. 16 we compare the state-dependent effective masses for the ^{3}He in the two ^{4}He thin films. The 3.14-layer results are in the top two panels, and the 4.33-layer results are in the bottom two panels. The data points on the zero-polarization

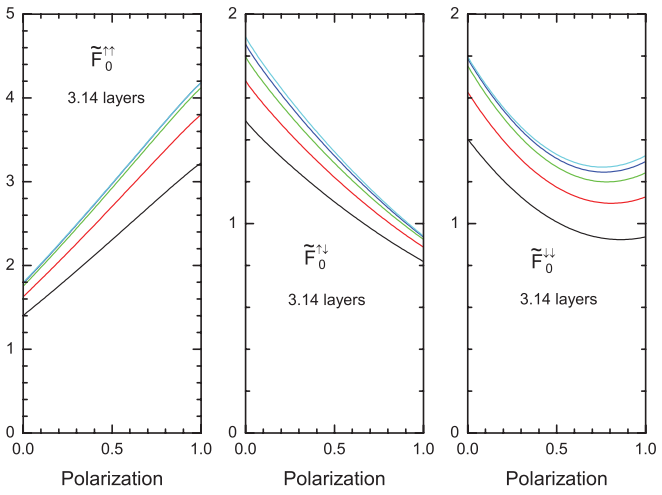

FIG. 12. (Color online) The Landau parameters $\tilde{F}_0^{\uparrow\uparrow}, \tilde{F}_0^{\uparrow\downarrow}$, and $\tilde{F}_0^{\downarrow\downarrow}$ for a thin ^{3}He film in a 3.14-layer ^{4}He film at five coverages as a function of polarization. In each figure the lowest curve corresponds to the lowest coverage, and the curves progress in order up to the highest curve at the highest coverage. The five coverages are $\overline{n} = 0.0128$, 0.0161, 0.0193, 0.0241, and 0.0289 Å^{-2}.

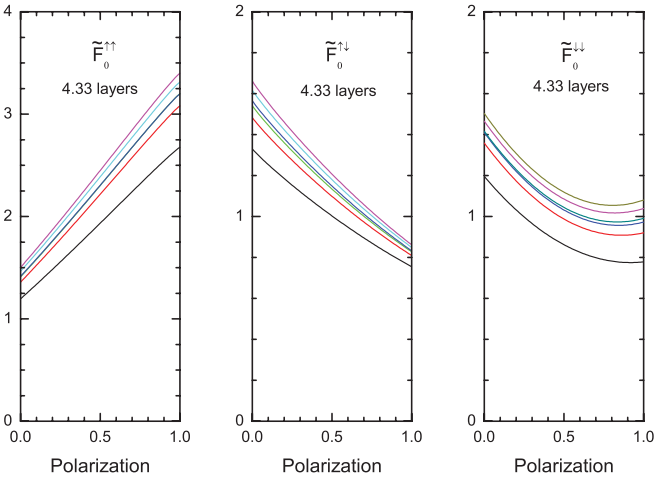

FIG. 14. (Color online) The Landau parameters $\tilde{F}_0^{\uparrow\uparrow}, \tilde{F}_0^{\uparrow\downarrow}$, and $\tilde{F}_0^{\downarrow\downarrow}$ for a thin ^{3}He film in a 4.33-layer ^{4}He film at six coverages as a function of polarization. In each figure the lowest curve corresponds to the lowest coverage, and the curves progress in order up to the highest curve at the highest coverage. The six coverages are $\overline{n} = 0.0153$, 0.0187, 0.0215, 0.0248, 0.0280, and 0.0311 Å^{-2}.

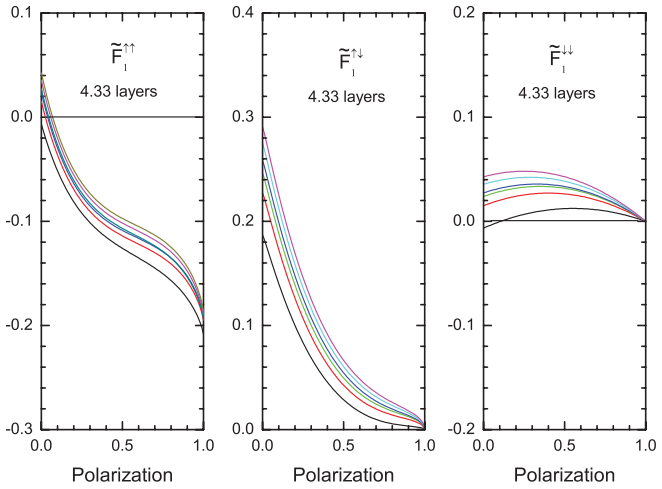

FIG. 15. (Color online) The Landau parameters $\tilde{F}_1^{\uparrow\uparrow}$, $\tilde{F}_1^{\uparrow\downarrow}$, and $\tilde{F}_1^{\downarrow\downarrow}$ for a thin ^{3}He film in a 4.33-layer ^{4}He film at six coverages as a function of polarization. In each figure the lowest curve corresponds to the lowest coverage, and the curves progress in order up to the highest curve at the highest coverage. The six coverages are $\overline{n} = 0.0153$, 0.0187, 0.0215, 0.0248, 0.0280, and 0.0311 Å^{-2}.

ordinates in all the panels are the fits from experiment as described above. From experiment, the effective masses dramatically increase in magnitude with increasing areal density. The qualitative differences between these results and those on graphite Fig. 5 are due to the smaller maximum density for the film data as discussed above. Also note that for the mixture film the effective mass is measured relative to the hydrodynamic mass $m_{\rm H}$ and not the bare mass m. The hydrodynamic mass as a function of ^{4}He film thickness was determined in Ref. 35. For theoretical discussions of the hydrodynamic mass see Ref. 36. These systems also show the same tendency for $m_\uparrow^*/m_H < 1$ in the large polarization limit

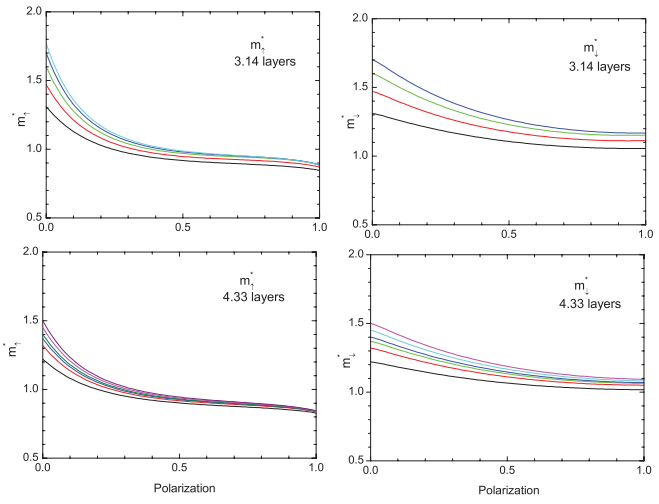

FIG. 16. (Color online) The spin-up and spin-down effective masses $m_\sigma^*/m_{\rm H}$ for a thin ^{3}He film in mixture films of 3.14 ^{4}He layers (top) and 4.33 layers (bottom) as a function of polarization. Note that the specific ^{3}He coverages for the two film thicknesses are not identical. In the limit of large polarization we find $m_\uparrow^*/m < 1$ as was also the case for the graphite substrate.

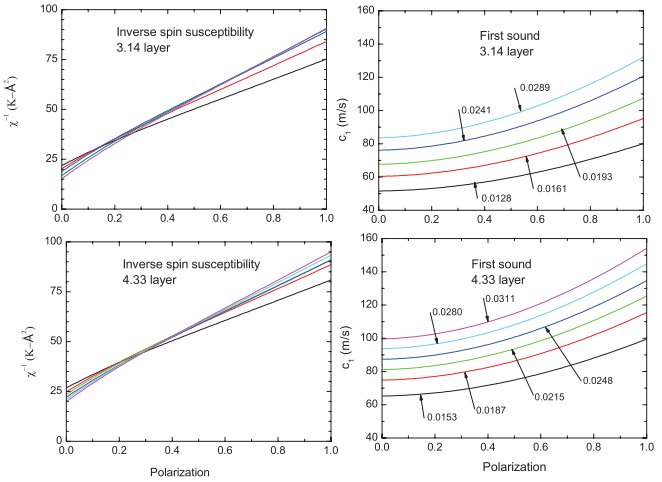

FIG. 17. (Color online) The inverse spin susceptibility χ^{-1} and the first sound speed c_1 for ^{3}He on a 3.14-layer ^{4}He film (top) and a 4.33-layer ^{4}He film (bottom). The five ^{3}He coverages for the 3.14-layer ^{4}He film and the six ^{3}He coverages for the 4.33-layer film are labeled in the first sound panels, and all are in units of Å^{-2}. The spin susceptibilities show the same small polarization crossing as the ^{3}He on graphite data (see Fig. 8). The first sound data (inverse square root of the compressibility) for the two films are very similar, with the thicker film showing a slightly larger stiffness.

as on the graphite substrate. The source of this behavior is the tendency for $\tilde{F}_1^{\uparrow\uparrow}$ to become large and negative with increasing polarization.

First sound speeds (essentially the inverse of the square root of the compressibility) and the inverse spin susceptibilities for the two ^{4}He film substrates are shown in Fig. 17, right panels and left panels, respectively. The inverse susceptibilities have the same tendency to cross at low polarization as seen in the graphite substrate data (Fig. 8). At low polarization, the smallest areal density film has the smallest spin susceptibility. At high polarization the largest areal density film has the smallest spin susceptibility. For both films, the crossing seems to be close to a single point at approximately 30% polarization. In any case, the effect is not large, and the spin susceptibility is to first order not sensitive to ^{3}He coverage. The polarization and ^{3}He coverage dependence of the compressibility in terms of the first sound speed is similar to that shown previously in Fig. 7. The incompressibility increases monotonically with both increasing ^{3}He coverage (positive compressibility for film stability) and also with increasing polarization.

The polarization and ^{3}He coverage dependence of the zero-sound speeds for the two ^{4}He film substrates are shown in Fig. 18. The zero-sound speeds for the 4.33-layer film are slightly larger than those for the 3.14-layer film for a given polarization and ^{3}He coverage. We believe that this difference is largely an effective mass effect. Essentially, the thinner film with the larger effective mass has a smaller Fermi velocity. We note that the zero-sound speeds are slightly larger than their respective first sound speeds shown in Fig. 17. This relationship $c_0 > c_1$ at a given density and polarization is the same as on the graphite substrate (see Figs. 10 and 7) and also in bulk ^{3}He.[29] In spite of the fact that these results are quite reasonable, we do need to emphasize that the differences in

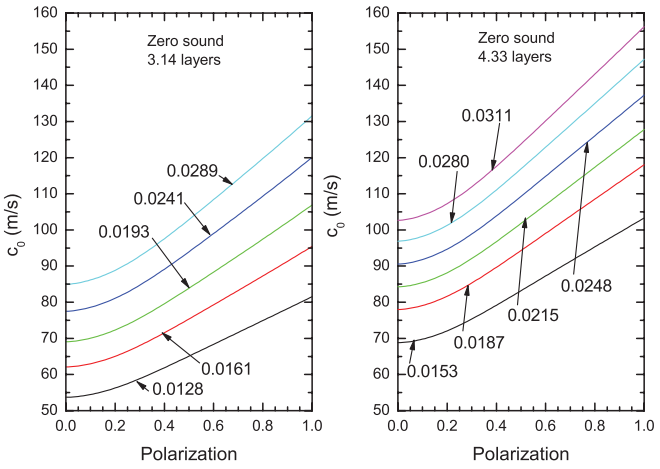

FIG. 18. (Color online) Zero-sound speeds for ^{3}He in 3.14 layers of ^{4}He (left) and 4.33 layers of ^{4}He (right). The five ^{3}He coverages for the 3.14-layer ^{4}He film and the six ^{3}He coverages for the 4.33-layer ^{4}He film are all in units of Å^{-2}.

our calculated c_0's and c_1's are very small in some cases, and we doubt that our theory can allow us to conclude definitively that $c_0 > c_1$ for all polarizations and substrates in the density ranges that we investigated.

VI. CONCLUSION

In this paper, we have used Fermi liquid theory to study the thermodynamic properties of thin, arbitrarily polarized ^{3}He films. Exact, analytic expressions for the Landau parameters were obtained from a recent[14] perturbation theoretic calculation of the ground-state energy of a two-dimensional many-fermion system to quadratic order in the s-wave and p-wave effective interaction parameters. The values of these parameters are obtained by fitting existing effective mass and spin susceptibility measurements in systems of second-layer ^{3}He on graphite, and also ^{3}He-^{4}He thin mixture films. An important advantage of fitting the underlying interaction parameters directly instead of the state-dependent Landau parameters is the ability to compute the angular components of the Landau parameters to all orders. The basic assumption that we make is that the low-density energy expression is a reasonable model at the moderate submonolayer coverages of interest. The main results of this paper are the fitted, effective s-wave and p-wave T-matrix components as functions of density, as shown in Fig. 1. We note in support of our basic assumption that the parameters show only modest dependence on density. Knowledge of the effective interaction parameters allows us to calculate the state-dependent Landau parameters and therefore the thermodynamic response and collective excitations in our systems. The allowed values of the Landau parameters are constrained by the issue of thermodynamic stability. In Sec. III C of this paper we derive the conditions that the Landau parameters must obey in order to ensure thermodynamic stability for an arbitrarily polarized Fermi liquid film.

For the mixture films there is an added complication due to the existence of a preferred frame of reference created by the superfluid rest frame. This is especially important for the bulk mixture.[23] It is not clear whether this is also important for this system where the ^{3}He is positioned on the outer edge of the ^{4}He film.[37] For the bulk system, BBP theory[38] that assumes a translationally invariant effective interaction is quite successful at describing the system. For the thin film mixtures we need to essentially follow BBP and to assume that it is reasonable to treat the effective interaction as local. Then the ^{4}He superfluid substrate is just the source of an enhanced effective mass for the ^{3}He in the zero concentration limit. The dominant excitations in these systems are, of course, the modified ripplons of the superfluid background.[39]

The thermodynamic quantities discussed in Sec. III A depend on the $\ell = 0,1$ angular components of the Landau parameters. In the following table we collect the values of the parameters in the important zero polarization limit. The Landau parameters $F_0^{\rm a}$ and $F_1^{\rm s}$ are determined by fitting the spin susceptibility and the effective mass, respectively. The values shown for $F_0^{\rm s}$ and $F_1^{\rm a}$ are predictions of this model. These Landau parameters, like all others in this paper, are normalized by a single spin-state density of states. If one wishes to compare our fitted values of $F_0^{\rm a}$ and $F_1^{\rm s}$ in Table I with those in the literature, then one simply needs to multiply these by a factor of two. There is a slight complication. In Refs. 4, 10, 32, and 37 there appears a superfluous factor of one-half as the coefficient of the F_1^s Landau parameter in the expression for the effective mass. By inspection of Eq. (3.5), it is clear that when using a two spin-state density of states to normalize the Landau parameters the coefficient of F_1^s should be one. This conclusion is in agreement with previous results of ERZ.[12] Thus, to compare our results with those in these and similar references, one must multiply the F_1^s entries in our Table I by a factor of four.

Figures 9 and 18 show that zero sound is a stable collective excitation for the entire polarization range at every density that we examined for both substrates. There is an important difference between zero sound on graphite and that in the mixture films that is due to the higher areal densities that

TABLE I. The $\ell = 0,1$ symmetric and antisymmetric Landau parameters for ^{3}He in two dimensions. Note that these are defined with the single spin state density of states $F_\ell^{\rm a,s} = (m^*/m)\tilde{F}_\ell^{\rm a,s}$.

Substrate	Density (Å^{-2})	$F_0^{\rm s}$	$F_0^{\rm a}$	$F_1^{\rm s}$	$F_1^{\rm a}$
Graphite	0.013	1.28	−0.25	0.15	−0.16
Graphite	0.025	2.66	−0.31	0.36	−0.28
Graphite	0.037	5.37	−0.36	0.82	−0.48
Graphite	0.046	8.35	−0.36	1.3	−0.67
Graphite	0.054	11.8	−0.40	1.9	−0.91
3.14 ^{4}He	0.013	1.90	−0.057	0.16	−0.13
3.14 ^{4}He	0.016	2.43	−0.041	0.24	−0.16
3.14 ^{4}He	0.019	2.84	−0.035	0.30	−0.19
3.14 ^{4}He	0.024	3.10	−0.060	0.35	−0.21
3.14 ^{4}He	0.029	3.26	−0.085	0.39	−0.23
4.33 ^{4}He	0.015	1.54	−0.082	0.11	−0.12
4.33 ^{4}He	0.019	1.88	−0.082	0.16	−0.14
4.33 ^{4}He	0.022	2.02	−0.090	0.19	−0.15
4.33 ^{4}He	0.025	2.09	−0.105	0.20	−0.16
4.33 ^{4}He	0.028	2.23	−0.110	0.23	−0.17
4.33 ^{4}He	0.031	2.37	−0.119	0.25	−0.19

are possible on graphite. The values of F_1^s in Table I for graphite at the highest densities become so large (due to the increase in the effective mass) that the cross term in Eq. (3.19) becomes appreciable. Thus, at these higher densities the "simplest approximation" of ignoring contributions to the zero-sound expressions from Landau parameters with $\ell \geqslant 1$ becomes highly inaccurate. This effect is largest at small polarizations and is mitigated somewhat at large polarizations. At zero polarization the stability of the zero-sound mode is due to the fairly large value of F_0^s. Likewise, the instability of the spin-zero-sound mode is due to the small and negative value of F_0^a. We note that the increase in the speed of the zero-sound mode as a function of polarization in the small polarization region is in agreement with the results of Ref. 40. Our results indicate that zero sound will propagate at all polarizations and that spin-zero-sound will not propagate in any of these thin film systems. In Fig. 11 we show explicitly the angular distortion of the Fermi surface in the presence of a zero-sound excitation.

^{3}He films are formed on a substrate and therefore their collective motion is determined by the relative size of the film thickness compared to the viscous penetration depth δ.[41] The viscous penetration depth is defined by $\delta = \sqrt{2\eta/\omega\rho}$, where η is the first viscosity, ρ is the mass density, and ω is the frequency. For typical experiments δ tends to be many times larger than the film thickness. Thus, the hydrodynamic normal fluid velocity is "clamped" at the substrate, and long-wavelength collective excitations do not propagate. Nevertheless even without a large Q the excitations are present, and can be probed. In a recent neutron scattering experiment, Godfrin *et al.*[42] were able to measure the phase velocity of zero sound at a single ^{3}He film thickness, energy, and wave vector. Their substrate was graphite, the ^{3}He areal density was $\overline{n} = 0.049$ Å^{-2}, the wave vector was $q = 5.5$ nm^{-1}, and the energy transfer was $\omega = 0.68 \pm 0.05$ meV. This yields a zero-sound speed of $c_0 \approx 190 \pm 14$ m/s. Our predicted results as shown in Fig. 10 in Sec. IV are in satisfactory agreement. We find a calculated zero-sound speed for this system of $c_0 = 181$ m/s.

The strong drops in the effective mass as a function of polarization at higher coverages on the graphite substrate are apparent from Fig. 5. This seems to be the most dramatic polarization-dependent behavior predicted from this model. For the mixture film system the predicted decreases in the effective mass are less pronounced, as can be seen in Fig. 16, since the maximum ^{3}He coverage is much smaller here than on graphite. Our model also predicts that in the limit of large polarization $m_\uparrow^*/m < 1$ because of the large negative values taken on by $\tilde{F}_1^{\uparrow\uparrow}$. For each of the substrates this model predicts that at a given density the polarization dependence of the inverse spin susceptibilities cross over at around 10% polarization with the smallest density having the largest susceptibility at high polarizations. This predicted behavior might be an important clue as to how to achieve maximum polarization in the ^{3}He film system. We note that, unlike in three dimensions, the spin susceptibility decreases monotonically with increasing polarization but does not vanish at full polarization. In all of the systems, the compressibility decreases as a function of polarization at fixed density.

These results are all predictions. Testing these predictions will be difficult since polarizing the ^{3}He system means ordering a *nuclear* moment. However, for the ultracold gases nonzero polarization is not a critical issue. There has been considerable recent progress in preparing ultracold Fermi gas systems in quasi-two-dimensional configurations.[43] These systems can be controlled in a weakly bound lateral trap and a strongly bound transverse trap. In the limit that the Fermi energy of the trapped atoms is small relative to the lateral trap single-particle energy spacing, we expect that the theory presented here is applicable. Further, even if there is imposed a lateral periodic potential then as long as the density is small enough so that only one Bloch band is occupied, the theory presented here should be applicable. At this time there do not appear to have been any measurements of thermodynamic quantities or collective excitations.

The question of attenuation of zero sound and first sound as a function of polarization in thin Fermi liquid films will be addressed in a future publication. In addition, we are still examining the interesting question of whether there is a Mermin's theorem[44] in a Fermi liquid with a finite polarization. The numerically obtained solutions of Eq. (3.22) always have one real root with magnitude greater than 1.

*zhaozhe.li@email.wsu.edu
†rha@spu.edu
‡mdm@wsu.edu

[1] J. G. Dash, *Films on Solid Surfaces* (Academic Press, New York, 1975).
[2] M. Bretz, J. G. Dash, D. C. Hickernell, E. O. McLean, and O. E. Vilches, Phys. Rev. A **8**, 1589 (1973); D. C. Hickernell, E. O. McLean, and O. E. Vilches, Phys. Rev. Lett. **28**, 789 (1972); S. W. Van Sciver and O. E. Vilches, Phys. Rev. B **18**, 285 (1978).
[3] D. S. Greywall, Phys. Rev. B **41**, 1842 (1990).
[4] C. P. Lusher, B. P. Cowan, and J. Saunders, Phys. Rev. Lett. **67**, 2497 (1991); M. Dann, J. Nyéki, B. P. Cowan, and J. Saunders, *ibid.* **82**, 4030 (1999).
[5] H. Godfrin and H.-J. Lauter, in *Progress in Low Temperature Physics*, edited by W. P. Halperin (Elsevier, Amsterdam, 1995), Vol. XIV, Chap. 4.
[6] R. B. Hallock, in *Progress in Low Temperature Physics*, edited by W. P. Halperin (Elsevier, Amsterdam, 1995), Vol. XIV, Chap. 5.
[7] L. D. Landau, Zh. Eskp. Teor. Fiz. **30**, 1058 (1956) [Sov. Phys. JETP **3**, 920 (1957)]; **32**, 59 (1957) [Sov. Phys. JETP **5**, 101 (1957)].
[8] L. D. Landau, Zh. Eskp. Teor. Fiz. **35**, 97 (1958) [Sov. Phys. JETP **8**, 70 (1959)].
[9] P. Bloom, Phys. Rev. B **12**, 125 (1975).
[10] S. M. Havens-Sacco and A. Widom, J. Low Temp. Phys. **40**, 357 (1980).
[11] V. M. Galitskii, Zh. Eskp. Teor. Fiz. **34**, 151 (1958) [Sov. Phys. JETP **7**, 104 (1958)].
[12] J. R. Engelbrecht, M. Randeria, and L. Zhang, Phys. Rev. B **45**, 10135 (1992).
[13] A. A. Abrikosov and I. M. Khalatnikov, Zh. Eskp. Teor. Fiz. **33**, 1154 (1957) [Sov. Phys. JETP **6**, 888 (1958)].
[14] R. H. Anderson and M. D. Miller, Phys. Rev. B **84**, 024504 (2011).

[15]K. S. Bedell and K. F. Quader, Phys. Lett. A **96**, 91 (1983); K. F. Quader and K. S. Bedell, J. Low Temp. Phys. **58**, 89 (1985).
[16]D. J. Thouless, *The Quantum Mechanics of Many-Body Systems*, 2nd ed. (Academic Press, New York, 1972).
[17]H.-T. Tan and E. Feenberg, Phys. Rev. **176**, 370 (1968).
[18]E. Krotscheck, AIP Conf. Proc. **103**, 132 (1983).
[19]M. Randeria, J.-M. Duan, and L.-Y. Shieh, Phys. Rev. B **41**, 327 (1990).
[20]M. Abramowitz and I. A. Stegun (editors), *Handbook of Mathematical Functions with Formulas, Graphs, and Mathematical Tables* (Dover, New York, 1965).
[21]P. Nozières and J. M. Luttinger, Phys. Rev. **127**, 1423 (1962); J. M. Luttinger and P. Nozières, *ibid.* **127**, 1431 (1962).
[22]K. S. Bedell, in *Proceedings of the Third International Conference on Recent Progress in Many Body Theories*, edited by H. Kümmel and M. L. Ristig, Lecture Notes in Physics, Vol. 198 (Springer, New York, 1984), pp. 200–209.
[23]G. Baym and C. Pethick, *Landau Fermi-Liquid Theory* (Wiley, New York, 1991).
[24]R. H. Anderson and M. D. Miller, J. Low Temp. Phys. **134**, 625 (2004) [Erratum: Eqs. (5), (7), and (17) should contain a factor of π and not π^2].
[25]D. Pines and P. Nozières, *The Theory of Quantum Liquids* (Benjamin, New York, 1966).
[26]I. M. Khalatnikov and A. A. Abrikosov, Zh. Eskp. Teor. Fiz. **33**, 110 (1957) [Sov. Phys. JETP **6**, 84 (1958)].
[27]I. Ia. Pomeranchuk, Zh. Eskp. Teor. Fiz. **35**, 524 (1958) [Sov. Phys. JETP **8**, 361 (1958)].
[28]H. Akimoto, J. D. Cummings, and R. B. Hallock, Phys. Rev. B **73**, 012507 (2006).
[29]W. R. Abel, A. C. Anderson, and J. C. Wheatley, Phys. Rev. Lett. **17**, 74 (1966).
[30]M. J. DiPirro and F. M. Gasparini, Phys. Rev. Lett. **44**, 269 (1980); **44**, 835 (1980); B. Bhattacharyya and F. M. Gasparini, *ibid.* **49**, 919 (1982); F. M. Gasparini, B. Bhattacharyya, and M. J. DiPirro, Phys. Rev. B **29**, 4921 (1984); B. K. Bhattacharyya, M. J. DiPirro, and F. M. Gasparini, *ibid.* **30**, 5029 (1984); B. K. Bhattacharyya and F. M. Gasparini, *ibid.* **31**, 2719 (1985).
[31]J. M. Valles, R. H. Higley, B. R. Johnson, and R. B. Hallock, Phys. Rev. Lett. **60**, 428 (1988); R. H. Higley, D. T. Sprague, and R. B. Hallock, *ibid.* **63**, 2570 (1989); N. Alikacem, D. T. Sprague, and R. B. Hallock, *ibid.* **67**, 2501 (1991); D. T. Sprague, N. Alikacem, P. A. Sheldon, and R. B. Hallock, *ibid.* **72**, 384 (1994).
[32]P.-C. Ho and R. B. Hallock, Phys. Rev. Lett. **87**, 135301 (2001).
[33]J. Cummings, H. Akimoto, and R. B. Hallock, J. Low Temp. Phys. **138**, 325 (2005).
[34]R. H. Anderson, M. D. Miller, and R. B. Hallock, Phys. Rev. B **59**, 3345 (1999).
[35]D. T. Sprague, N. Alikacem, and R. B. Hallock, Phys. Rev. Lett. **74**, 4479 (1995).
[36]B. E. Clements, E. Krotscheck, and M. Saarela, J. Low Temp. Phys. **100**, 175 (1995); E. Krotscheck, J. Paaso, M. Saarela, and K. Schörkhuber, Phys. Rev. B **64**, 054504 (2001).
[37]E. Krotscheck, M. Saarela, and J. L. Epstein, Phys. Rev. B **38**, 111 (1988).
[38]J. Bardeen, G. Baym, and D. Pines, Phys. Rev. Lett. **17**, 372 (1966); Phys. Rev. **156**, 207 (1967).
[39]E. Krotscheck and M. D. Miller, Phys. Rev. B **73**, 134514 (2006).
[40]M. T. Béal-Monod, O. T. Valls, and E. Daniel, Phys. Rev. B **49**, 16042 (1994).
[41]S. J. Putterman, *Superfluid Hydrodynamics* (North-Holland, Amsterdam, 1974).
[42]H. Godfrin, M. Meschke, H.-J. Lauter, H. Böhm, E. Krotscheck, and M. Panholzer, J. Low Temp. Phys. **158**, 147 (2010).
[43]K. Günter, T. Stöferle, H. Moritz, M. Köhl, and T. Esslinger, Phys. Rev. Lett. **95**, 230401 (2005); K. Martiyanov, V. Makhalov, and A. Turlapov, *ibid.* **105**, 030404 (2010); B. Fröhlich, M. Feld, E. Vogt, M. Koschorreck, W. Zwerger, and M. Köhl, *ibid.* **106**, 105301 (2011); A. T. Sommer, L. W. Cheuk, M. J. H. Ku, W. S. Bakr, and M. W. Zwierlein, *ibid.* **108**, 045302 (2012).
[44]N. D. Mermin, Phys. Rev. **159**, 161 (1967).